




DOMAIN 2 CELL ARCHITECTURE AND GROWTH

Structure, Assembly, and Function of Flagella Responsible for Bacterial Locomotion

 TOHRU MINAMINO^a AND MIKI KINOSHITA^a

^aGraduate School of Frontier Biosciences, Osaka University, Suita, Osaka, Japan

Received: 18 January 2023

Accepted: 14 April 2023

Published: 1 June 2023

Editor: James M. Slauch, University of Illinois at Urbana-Champaign

Address correspondence to Tohru Minamino, tohru@fbs.osaka-u.ac.jp.

Copyright: © 2023 American Society for Microbiology. All Rights Reserved.

ABSTRACT Many motile bacteria use flagella for locomotion under a variety of environmental conditions. Because bacterial flagella are under the control of sensory signal transduction pathways, each cell is able to autonomously control its flagellum-driven locomotion and move to an environment favorable for survival. The flagellum of *Salmonella enterica* serovar Typhimurium is a supramolecular assembly consisting of at least three distinct functional parts: a basal body that acts as a bidirectional rotary motor together with multiple force generators, each of which serves as a transmembrane proton channel to couple the proton flow through the channel with torque generation; a filament that functions as a helical propeller that produces propulsion; and a hook that works as a universal joint that transmits the torque produced by the rotary motor to the helical propeller. At the base of the flagellum is a type III secretion system that transports flagellar structural subunits from the cytoplasm to the distal end of the growing flagellar structure, where assembly takes place. In recent years, high-resolution cryo-electron microscopy (cryoEM) image analysis has revealed the overall structure of the flagellum, and this structural information has made it possible to discuss flagellar assembly and function at the atomic level. In this article, we describe what is known about the structure, assembly, and function of *Salmonella* flagella.

KEYWORDS bacterial flagellum, chemotaxis, cryoEM image analysis, energy coupling, flagellar assembly, flagellar gene regulation, motility, torque generation, transmembrane proton channel, type III secretion system

The bacterial flagellum is a supramolecular protein complex with a strictly defined morphology and is one of the organelles responsible for bacterial locomotion under a variety of environmental conditions. Because the overall structure of the bacterial flagellum and its mechanical function are highly conserved among bacterial species, *Escherichia coli* and *Salmonella enterica* serovar Typhimurium (referred to as *Salmonella* here) are considered model organisms that provide deep insights into the structure, assembly, and function of the bacterial flagellum (1, 2).

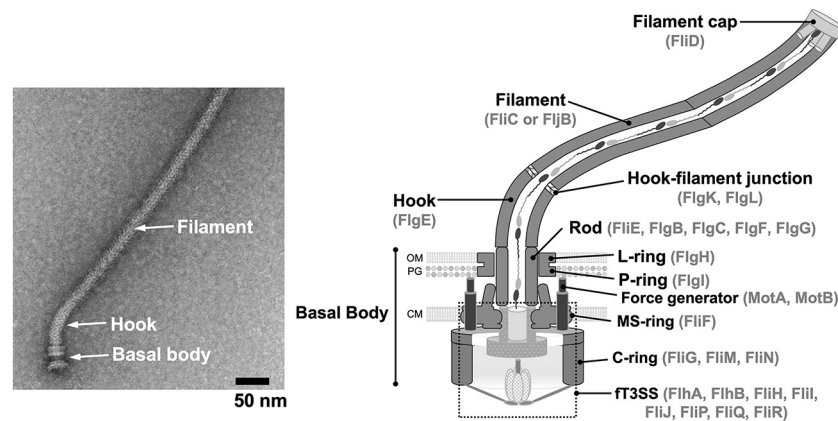


FIG 1 The *Salmonella* flagellum. An electron micrograph of the flagellum isolated from *Salmonella* (left) and its schematic diagram (right) are shown. The flagellum is divided into at least three distinct functional parts: a basal body that is a bidirectional rotary motor, a hook that functions as a universal joint, and a filament that acts as a helical propeller. A hook-filament junction connects the hook and filament. A filament cap is located at the tip of the filament and facilitates filament assembly. To construct the flagellum beyond the cytoplasmic membrane, flagellar structural subunits are translocated via a type III secretion system (ft3SS) that is located at the base of the flagellum and assemble at the tip of the growing structure. Several force generators surround the basal body. OM, outer membrane; PG, peptidoglycan layer; CM, cytoplasmic membrane.

The flagellum of *Salmonella* consists of about 30 different proteins with copy numbers ranging from a few to tens of thousands and is divided into three distinct functional parts: a basal body, a hook, and a filament (Fig. 1 and Table 1). The basal body is located within the cell envelope and functions as a bidirectional rotary motor together with multiple MotA₅-MotB₂ complexes, each of which serves as a force generator. The *Salmonella* flagellar motor is powered by a transmembrane electrochemical gradient of protons (H⁺), namely, proton motive force (PMF) (note that many motile bacteria such as marine *Vibrio* and extremely alkalophilic *Bacillus* bacteria use sodium ions [Na⁺] to drive the rotation of their flagellar motors, with the PomA₅-PomB₂ complex in the *Vibrio* flagellar motor and the MotP₅-MotS₂ complex in *Bacillus*). The hook and filament are present on the outside of the cell body. The filament acts as a helical propeller that generates thrust to propel the cell body, while the hook is located between the basal body and the filament and functions as a universal joint that transmits the torque produced by the rotary motor to the helical propeller (3–5).

Salmonella cells produce multiple flagella (typically about 5 to 10 per cell) from random locations on the cell surface. Each rotary motor has a directional switching device that allows it to rotate in both counterclockwise (CCW) (viewed

from the flagellar filament to the motor) and clockwise (CW) directions. When all of the motors rotate in the CCW direction, long helical filaments form a bundle structure behind the cell body, generating enough thrust for the cell to swim in a straight line. When one or more motors switch the direction of rotation from CCW to CW, the bundle structure is disrupted, allowing the cell to tumble and change swimming direction. The switching device is under the control of sensory signal transduction pathways, allowing each *Salmonella* cell to sense changes in chemicals in its environment and to move closer to stimuli that are favorable for survival and away from those that are unfavorable (6).

Flagellar assembly begins with the basal body, followed by the hook and, finally, the filament. To construct multiple flagella on the cell surface of *Salmonella*, flagellar structural subunits pass the cytoplasmic membrane via the flagellar type III secretion system (ft3SS) located at the base of each flagellum, diffuse through a narrow central channel, and assemble at the distal end of the growing flagellar structure (Fig. 1). To terminate hook assembly and initiate filament assembly at a specific stage of the hook structure, the ft3SS transports a ruler protein secreted during hook assembly, which not only measures the hook length but also switches the substrate specificity of the ft3SS (7, 8).

TABLE 1 Proteins involved in the flagellation and motility of *Salmonella*

Protein	Mol mass (kDa)	Function(s)	UniProt accession no.
Proteins involved in the structure and assembly of the basal body rings			
FliF	61.2	MS ring, rotor	P15928
FliG	36.9	C ring, rotor, directional switch	P0A1J9
FliM	37.9	C ring, rotor, directional switch	P26418
FliN	14.8	C ring, rotor, directional switch	P26419
FlgH	22.4 (24.7 ^a)	L ring, bushing	P0A1N8
FlgI	36.3 (38.2 ^a)	P ring, bushing	P15930
FlgA	21.3 (23.6 ^a)	Periplasmic chaperone for P-ring assembly	P40131
Proteins involved in the structure and assembly of the flagellar axial structure			
FliE	11.1	Proximal rod, structural adaptor that firmly connects the MS ring and rod	P26462
FlgB	15.1	Proximal rod	P16437
FlgC	14.0	Proximal rod	P0A1I7
FlgF	26.1	Proximal rod	P16323
FlgG	27.8	Distal rod	P0A1J3
FlgJ	34.4	Rod cap, muramidase	P15931
FlgD	24.0	Hook cap	P0A1I9
FlgE	42.2	Hook	P0A1J1
FliK	41.8	Secreted molecular ruler, export switch	P26416
FlgK	59.1	HAP1, hook-filament junction, structural adaptor connecting the hook and filament	P0A1J5
FlgL	34.2	HAP3, hook-filament junction, structural adaptor connecting the hook and filament	P16326
FliD	49.8	HAP2, filament cap	P16328
FliC	51.6	H1 flagellin, filament	P06179
FljB	52.5	H2 flagellin, filament	P52616
FliB	45.4	Lysine- <i>N</i> -methylase	Q56106
Proteins involved in the structure and assembly of the FT3SS			
FlhA	74.8	Export gate complex, dual-fuel export engine, substrate recognition, export switch	P40729
FlhB	42.4	Export gate complex, substrate recognition, export switch, opening and closing of the export gate	P40727
FliO	13.1	Scaffold for the assembly of the FliP-FliQ-FliR complex	P0A1L1
FliP	24.5 (26.8 ^a)	Export gate complex, polypeptide channel	P54700
FliQ	9.6	Export gate complex, polypeptide channel	P0A1L5
FliR	28.9	Export gate complex, polypeptide channel	P54702
FliH	25.8	ATPase ring complex, peripheral stalk	P15934
FliI	49.3	ATPase ring complex, ATP hydrolysis reaction	P26465

(Continued on next page)

TABLE 1 (Continued)

Protein	Mol mass (kDa)	Function(s)	UniProt accession no.
FliJ	17.3	ATPase ring complex, central stalk	P0A1K1
FlgN	16.0	Export chaperone specific for FlgK (HAP1) and FlgL (HAP3), translational control of FlgM	P0A1J7
FliS	14.7	Export chaperone specific for FliC, negative regulation of FlgM secretion	P26609
FliT	13.7	Export chaperone specific for FliD (HAP2), negative regulation of flagellar gene expression	P0A1N2
Proteins involved in force generation			
MotA	32.1	Transmembrane proton channel, direct interaction with FliG for force generation as well as stator assembly around the flagellar motor	P55891
MotB	34.2	Transmembrane proton channel, binding to the PG layer	P55892
Proteins involved in the control of gene expression			
FlhC	21.6	Positive regulator of class 2 gene expression	O52222
FlhD	13.0	Positive regulator of class 2 gene expression	P0A2R2
FliA	27.5	Flagellum-specific sigma factor (σ^{28}) for class 3 gene expression	P0A2E8
FliZ	21.7	Positive regulator of flagellar gene expression	P0A210
FlgM	10.6	Anti-sigma factor	P26477
FljA	20.3	Repressor of FliC expression	P52619
Hin	21.4	DNA invertase	P03013

^aMolecular mass of the precursor form before the cleavage of the signal peptide.

The overall structure of the flagellum has been revealed by high-resolution cryo-electron microscopy (cryoEM) image analyses (Fig. 2), so its assembly and mechanical function are now being understood at the atomic level (9–15). In this review article, we describe our current understanding of the structure, assembly, and function of the *Salmonella* flagellum.

THE FLAGELLAR STRUCTURE AND ITS MECHANICAL FUNCTION

The bacterial flagellum is divided into five distinct structural parts: a basal body, a hook, a hook-filament junction, a filament, and a filament cap. The basal body consists of the C ring, the MS ring, the P ring, the L ring, and the rod. The rod, the hook, the hook-filament junction, the filament, and the filament cap are called axial structures of the flagellum (Fig. 1). The basal body not only contains the σ^{28} to construct these axial structures beyond the cellular membranes but also accommodates multiple force generators around the MS ring to act as a bidirectional rotary motor (16, 17).

Structure and function of the flagellar basal body rings.

(i) MS ring. FliF is a transmembrane protein with two transmembrane helices (TMHs) and self-assembles into the MS ring in the cytoplasmic membrane (18, 19). The MS ring is both the structural template for assembling the C ring and the housing for the transmembrane export gate complex of the σ^{28} (20). Thus, the MS ring is the base for flagellar structure, assembly, and function. The MS ring had been believed to have 26-fold rotational symmetry for a long time (21). However, recent high-resolution cryoEM image analyses have shown that the MS ring in the native basal body is formed by 34 FliF subunits (Fig. 3A) (22–24). The lower half of the M ring is buried in the cytoplasmic membrane, and the S ring and the cylindrical collar are exposed to the periplasmic space. The periplasmic domain of FliF (FliF_p) (residues 47 to 454) has three globular domains, D1 (residues 60 to 124), D2 (residues 125 to 215), and D3 (residues 228 to 270 and residues 382 to 438), and a long, extended up-and-down structure, including two antiparallel β -strands (residues 271 to 381). The S ring is formed by 34 D3 domains of FliF_p horizontally packed

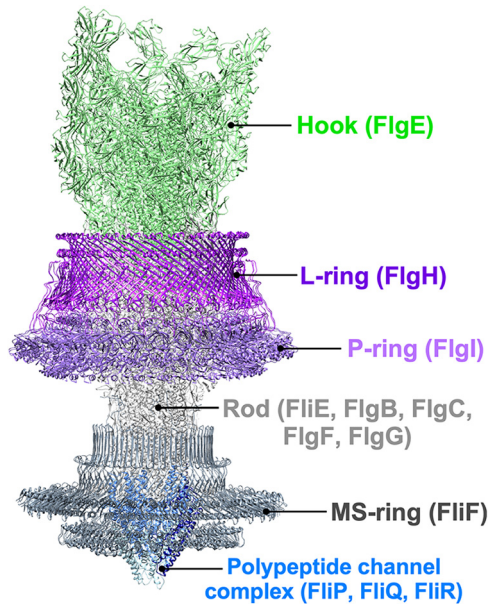


FIG 2 CryoEM structure of the *Salmonella* hook-basal body. Atomic model of the *Salmonella* native hook-basal body structure in C_{α} ribbon representation (PDB accession number 7CGO). The atomic model of the basal body consists of the MS ring (FliF) (slate gray); the P ring (FlgI) (medium purple); the L ring (FlgH) (purple); the polypeptide channel complex formed by FliP (cornflower blue), FliQ (light blue), and FliR (navy blue); and the rod (light gray). The hook (FlgE) (light green) is connected directly to the rod.

with their major axes oriented in the radial direction. The long β -hairpins in the upper part of the collar are vertically lined up to form a 68-stranded cylindrical β -barrel structure. Interestingly, the middle and inner parts of the M ring show two additional distinct symmetries. The inner part of the M ring is a flat ring with 23-fold rotational symmetry, and the middle part just outside the inner core ring shows a cog-like structure with 11-fold rotational symmetry, indicating that the MS ring is formed by 34 FliF subunits with two distinct conformations. Consistently, the crystal structure of the D1 and D2 domains of FliF_P derived from *Aquifex aeolicus* adopts two distinct conformations (25, 26). The FliP₅-FliQ₄-FliR₁ complex of the σ^{70} is located inside the central pore of the inner-core ring of the M ring. Therefore, it is likely that conformational changes in the D1 and D2 domains of FliF_P are important for creating a central pore of a suitable size to accommodate the FliP₅-FliQ₄-FliR₁ complex in the center of the M ring.

(ii) C ring. The C ring not only is part of the rotor of the flagellar motor but also serves as a direction-switching device

that allows the motor to rotate in both the CCW and CW directions (27–29). FliG, FliM, and FliN assemble into the C ring on the cytoplasmic surface of the MS ring (Fig. 4A) (30, 31). The C ring has 34-fold rotational symmetry, as does the MS ring (32–34). FliG consists of three distinct domains, the N-terminal (FliG_N), middle (FliG_M), and C-terminal (FliG_C) domains (Fig. 4B) (35). FliG_C is further divided into three distinct parts: an N-terminal subdomain (FliG_{CN}), a C-terminal subdomain (FliG_{CC}), and a flexible hinge connecting these two subdomains. FliG_N binds directly to the C-terminal cytoplasmic domain of FliF (36–38). Intermolecular interactions between FliG_N and FliG_N and between FliG_M and FliG_{CN} are responsible for FliG ring formation (39–41). FliG_{CC} is directly involved in the interaction with the force generator protein MotA, not only in torque generation but also in the assembly of the MotA₅-MotB₂ complex around the rotor (42, 43). FliM is composed of an intrinsically disordered N-terminal region (FliM_N), a middle domain (FliM_M), and a C-terminal domain (FliM_C). FliM_C is very similar in sequence and structure to FliN (44, 45). FliM_M binds directly to FliG_M to form a continuous wall of the C ring (46). FliM_C and FliN form a doughnut-shaped heterotetramer with a stoichiometry of 1 FliM_C domain and 3 FliN subunits, and this FliM_C-FliN₃ complex forms a continuous spiral density along the circumference at the bottom edge of the C ring (47).

Although the C-ring structures of purified CCW and CW motors show 34-fold rotational symmetry, high-resolution live-cell imaging techniques have shown that the copy number of the FliM₁-FliN₃ complex in the CCW motor is about 1.3 times higher than that in the CW motor, indicating that *in vivo*, the CCW motor can accommodate more FliM₁-FliN₃ complexes in the C ring. Interestingly, switching the conformational state of the C ring from CCW to CW induces the dissociation from several weakly bound FliM₁-FliN₃ complexes from the C ring. This adaptive remodeling of the C-ring structure is thought to be critical for the fine-tuning of the chemotactic response to temporal changes in the environment (48–51).

Sensory signal transduction pathways control how often the flagellar motor switches rotation in response to temporal changes in the environment (6). In *Salmonella*, the C ring is placed in a default CCW state. The phosphorylated form of CheY (CheY-P), which acts as a chemotaxis signaling molecule, binds with high affinity to FliM_N and with low affinity to FliM_M and FliN in the C ring (52–54). As a result, the C ring switches its conformational state

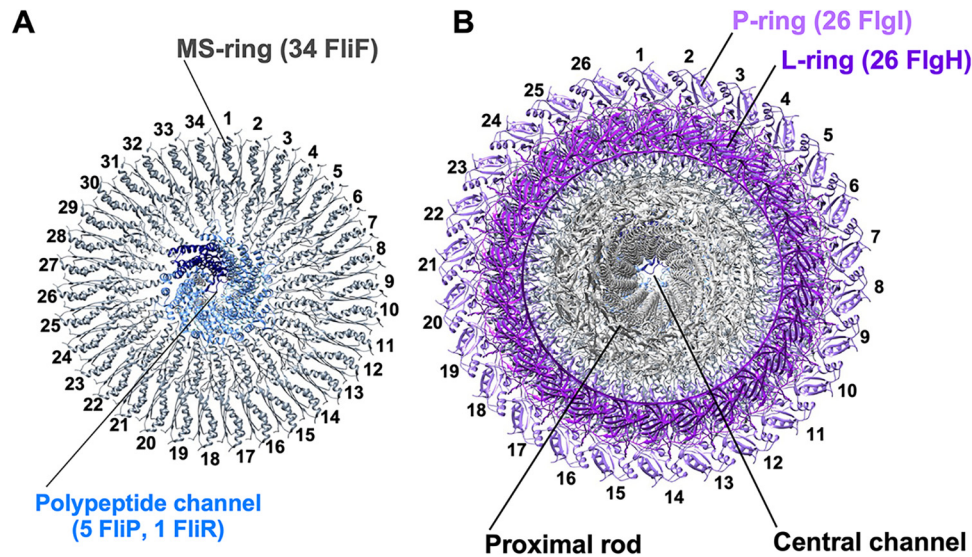


FIG 3 Rotational symmetry of basal body rings. (A) Vertical section of the atomic model of the S ring in C_α ribbon representation (PDB accession number 7CGO). FliF self-assembles into the MS ring with 34-fold rotational symmetry. The polypeptide channel complex with a stoichiometry of 5 FliP subunits, 4 FliQ subunits, and 1 FliR subunit is located inside the MS ring. FliP (cornflower blue) and FliR (navy blue) assemble into a helical structure inside the MS ring, and the central pore of the FliP₅-FliR₁ complex serves as a polypeptide channel that allows export substrates to be translocated across the cytoplasmic membrane. (B) Vertical section of the atomic model of the LP ring in C_α ribbon representation (PDB accession number 7CGO). The P ring (FlgI) (medium purple) and the L ring (FlgH) (purple) together form a very strong and stable ring complex with 26-fold rotational symmetry, and the LP ring acts as a molecular bushing for high-speed rod rotation inside it. The central channel of the axial structure is a physical pathway for the diffusion of the flagellar structural subunits in an unfolded conformation to the distal end of the growing flagellar structure.

from CCW to CW in a highly cooperative manner, allowing the motor to rotate in the CW direction. FliG_{CC} contains two conserved residues, Arg281 and Asp289, involved in the interaction with the MotA protein (Fig. 4B) (55, 56). The hinge connecting FliG_{CN} and FliG_{CC} has a flexible nature at the well-conserved MFXF motif, allowing FliG_{CC} to rotate 180° relative to FliG_{CN} to reorient the Arg281 and Asp289 residues in FliG_{CC} (Fig. 4C) (57). It has been reported that the binding of CheY-P to the C ring induces a tilting movement of FliM_M, resulting in the rotation of FliG_{CC} relative to FliG_{CN} (58). Thus, the MFXF motif is likely to serve as a gear changer of the flagellar motor.

FliG has two helix linkers, named Helix_{NM} and Helix_{MC} (Fig. 4B) (35). Helix_{MC} connecting FliG_M and FliG_{CN} is located at the interface between FliG_M and FliM_M and stabilizes the FliG_M-FliM_M interaction (Fig. 4D) (46, 59). Helix_{MC} also interacts with Helix_{NM} connecting FliG_N and FliG_M (35). Mutations located in and around the Helix_{NM} and Helix_{MC} linkers result in an unusual switching behavior of the flagellar motor, suggesting that these two helix

linkers are involved in the directional switching of the flagellar motor (29, 60). In-frame deletions of three residues, Pro169, Ala170, and Ala171, in the extreme N-terminal region of Helix_{MC} (CW-locked deletion) lock the motor into the CW state without CheY-P (61). The crystal structure of the FliG_M and FliG_C domains with the CW-locked deletion has shown that the CW-locked deletion not only induces conformational rearrangements of Helix_{MC} but also rotates FliG_{CC} relative to FliG_{CN} (Fig. 4D) (62). A homology model of *Salmonella* FliG built based on the crystal structure of FliG derived from *A. aeolicus* suggested that Thr103 of Helix_{NM} makes hydrophobic contacts with Pro169 and Ala173 of Helix_{MC} (Fig. 4B) (63). The T103S mutation in Helix_{NM} causes a strong CW switch bias (29), suggesting that a change in the Helix_{NM}-Helix_{MC} interaction mode is required for FliG_{CC} to rotate relative to FliG_{CN}. Since the CW-locked deletion causes the dissociation of Helix_{MC} from the FliG_M-FliM_M interface (Fig. 4D) (64), the binding of CheY-P to FliM and FliN in the C ring causes a conformational change at the FliG_M-FliM_M interface, not only dissociating Helix_{MC} from the interface but

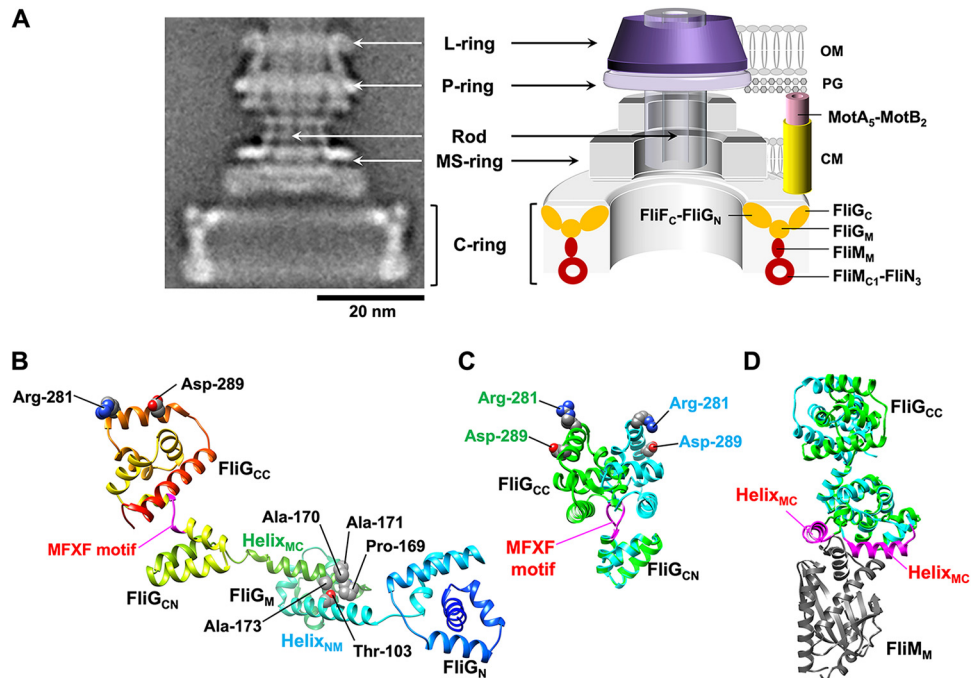


FIG 4 Structure of the C ring. (A) CryoEM image of the *Salmonella* basal body and its schematic diagram. The cryoEM image of the basal body in the left panel is modified from references [17](#) and [34](#) and is used here to provide a visual reference for the schematic diagram shown in the right panel. The basal body consists of the C ring, the MS ring, the P ring, the L ring, and the rod. There is no MotA₅-MotB₂ complex in the purified basal body (left), but multiple MotA₅-MotB₂ complexes are present around the MS-ring-C-ring complex and function as force generators for the flagellar motor (right). The C ring is composed of FliG, FliM, and FliN. The N-terminal domain of FliG (FliG_N) binds to the C-terminal cytoplasmic domain of FliF (FliF_C) to form the FliG ring on the cytoplasmic face of the MS ring. The C-terminal domain of FliG (FliG_C) is located in the upper part of the C ring. The middle domain of FliM (FliM_M) is located between the middle domain of FliG (FliG_M) and FliN and forms a continuous wall of the C ring. The continuous spiral density at the bottom edge of the C ring is made of the C-terminal domain of FliM (FliM_C) and FliN. OM, outer membrane; PG, peptidoglycan layer; CM, cytoplasmic membrane. (B) Homology model of *Salmonella* FliG built based on the crystal structure of FliG derived from *Aquifex aeolicus* (PDB accession number [3HJL](#)). The C_α backbone is color-coded from blue to red, going through the rainbow colors from the N to the C termini. FliG consists of three distinct FliG_N, FliG_M, and FliG_C domains and two helix linkers named Helix_{NM} and Helix_{MC}. FliG_C is divided into two distinct FliG_{CN} and FliG_{CC} subdomains. The highly conserved Arg281 and Asp289 residues in FliG_{CC} are responsible for interactions with the cytoplasmic domain of the MotA₅-MotB₂ complex. The conserved MFXF motif allows FliG_{CC} to rotate 180° relative to FliG_{CN}. Thr103 in Helix_{NM} interacts with Pro169 and Ala173 in Helix_{MC}. In contrast to the wild-type motor that is placed in a default CCW state, the in-frame deletion of three residues, Pro169, Ala170, and Ala171, locks the flagellar motor in the CW state. (C) Two distinct conformations of the FliG_C domain. Two distinct homology models of *Salmonella* FliG_C were built based on the structures of *Helicobacter pylori* FliG_C under PDB accession numbers [3USY](#) (green) and [3USW](#) (cyan). Conformational rearrangements of the conserved MFXF motif induce a 180° rotation of FliG_{CC} relative to FliG_{CN} to reorient the Arg281 and Asp289 residues. (D) Structural comparisons between the wild-type FliG_{MC} fragment composed of FliG_M, Helix_{MC}, and FliG_C (green) and its CW-locked variant (cyan). Homology models of the wild-type FliG_{MC}-FliI_M complex and the CW-locked form of FliG_{MC} were built based on the FliG_{MC}/FliI_M complex (PDB accession number [4FHR](#)) and the CW-locked FliG_{MC} variant (PDB accession number [3AJC](#)) derived from *Thermotoga maritima*, respectively. The FliG_M domain of the CW-locked variant is superimposed onto that of the FliG_{MC}/FliI_M complex. Helix_{MC} (magenta) is located at the interface between FliG_M and FliI_M (dark gray). In contrast, the CW-locked deletion not only induces a distinct orientation of Helix_{MC} relative to the FliG_M-FliI_M interface but also goes through a 90° rotation of FliG_{CC}.

also affecting the Helix_{NM}-Helix_{MC} interaction significantly. As a result, the C ring switches its conformational state from CCW to CW.

(iii) LP ring. The periplasmic protein FlgI assembles into the P ring within the peptidoglycan (PG) layer, and the lipoprotein FlgH forms the L ring within the outer membrane. The P ring and the L ring together form a cylindrical architecture with 26-fold rotational symmetry (Fig. 3B). The LP ring is very stable against various chemical treatments due to the complex intersubunit interactions of each subunit with up to six partners in the LP-ring structure. Because both the outer surface of the rod and the inner surface of the LP ring are very smooth and form a small gap between them that is large enough to accommodate one or two layers of water molecules in most of their interfaces, the LP ring can serve as a molecular bushing for the high-speed rotation of the rod acting as a driveshaft of the flagellar motor. The inner surface of the LP ring is charged both negatively and positively, whereas the outer surface of the rod is negatively charged, suggesting that both repulsive and attractive forces maintain the position of the rotating rod at the center of the LP ring (22, 23, 65).

FlgH and FlgI are synthesized as precursors with cleavable N-terminal signal peptides, which are cleaved as they pass through the cytoplasmic membrane (66). FlgI has an intramolecular disulfide bond, and the formation of this disulfide bond promotes the rapid protein folding of each FlgI monomer and protects it from degradation in the periplasmic space (67). The FlgI monomer requires the FlgA chaperone to assemble around the rod to form the P ring (68, 69). The P52L mutation in the distal rod protein FlgG not only produces abnormally elongated rods, called polyrods, but also allows the formation of many P rings around the polyrods (70). This suggests that the interaction between FlgG and FlgI must be properly controlled during P-ring formation around the rod. Two highly conserved residues, Lys63 and Lys95, of FlgI are located at the inner surface of the P ring and directly face a negative-charge cluster on the outer surface of the rod. Mutational analyses of these two Lys residues have shown that both Lys63 and Lys95 of FlgI are critical for efficient P-ring formation around the rod. These observations suggest that Lys63 and Lys95 of FlgI are essential for the initial binding of FlgI to the rod surface to form the P ring (65). Since the

L ring is not formed in *flgI*-null mutants, FlgH apparently requires P-ring formation around the rod to assemble into the L ring within the outer membrane. Because the P ring is tightly attached to the rod until the L ring is assembled above it, the interaction between FlgH and FlgI seems likely to cause conformational changes on the inner surface of the P ring (71, 72). As a result, the LP ring is free from the rod and acts as a bushing for the rapid and stable rotation of the rod with little friction (65).

Structure and function of the flagellar axial structure.

Flagellar axial proteins have a common structural motif at their N and C termini that forms an α -helical coiled coil in the inner-core D0 domain, and strong hydrophobic intermolecular interactions between these coiled coils make the axial structure mechanically stable (Fig. 5A). These terminal regions are intrinsically disordered in their monomeric state, preventing spontaneous assembly at inappropriate times and places. The rod (composed of FliE, FlgB, FlgC, FlgF, and FlgG), the hook (FlgE), the hook-filament junction (FlgK and FlgL), and the filament (FliC or FljB) form a helical tubular structure consisting of 11 protofilaments. The basic helical line that passes through all of the subunits is called the 1-start helix, and there are approximately 11 subunits per 2 turns of the 1-start helix (Fig. 5B). In contrast, the filament cap has 5-fold rotational symmetry (Fig. 6) (73).

(i) Rod. The rod is straight and rigid and acts as a driveshaft of the flagellar motor. The rod is divided into two structural parts: a proximal rod with a stoichiometry of 6 FliE, 5 FlgB, 6 FlgC, and 5 FlgF subunits and a distal rod consisting of 24 FlgG subunits (Fig. 7A) (22, 23, 74). For the construction of the proximal rod, FliE first assembles directly on the tip of the FliP₅-FliR₁ complex of the ft3SS to form the FliE zone with helical symmetry (Fig. 7B). FliE is composed of three α -helices, α 1, α 2, and α 3. Helices α 2 and α 3 of FliE form an α -helical coiled coil in the inner-core D0 domain, and each D0 domain of FliE binds to the FliP or FliR subunit. (Note: when FliE binds to FliR, helix α 2 is invisible, suggesting that helix α 3 does not form a coiled coil along with helix α 2.). Helix α 1 of FliE binds directly to the inner wall of the MS ring, allowing the rod to be tightly connected with the MS ring. Thus, the FliE zone acts as a mechanical adapter between the MS ring and the rod. FlgB and FlgC have two domains, D0 and Dc, while FlgF consists of three domains, D0, Dc, and D1. FlgB

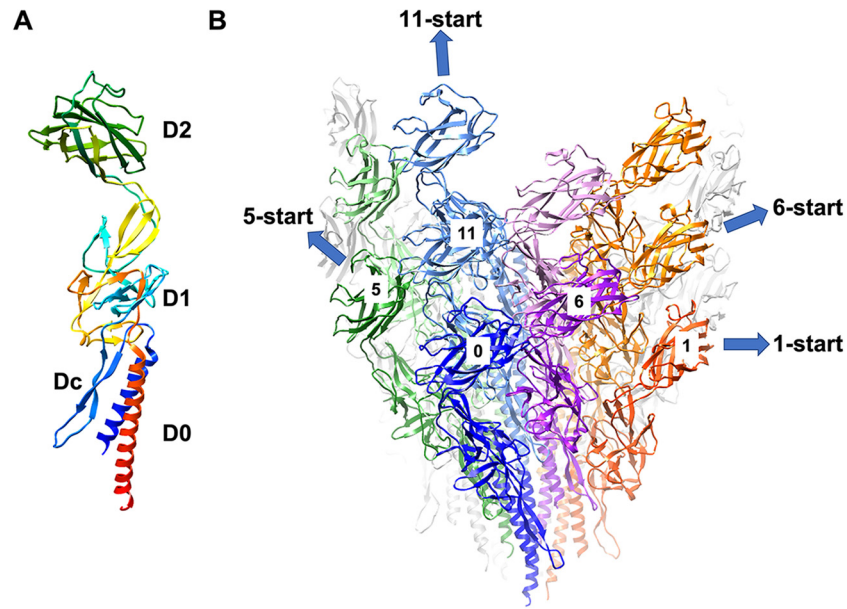


FIG 5 Common structural features of the flagellar axial structure. (A) Atomic model of the FlgE subunit in the hook structure (PDB accession number 7CGO). The C_α backbone is color-coded from blue to red, going through the rainbow colors from the N to the C termini. The N-terminal and C-terminal regions of FlgE are intrinsically disordered in its monomeric state, but when incorporated into the hook structure, they form an α -helical coiled coil in the inner-core D0 domain. (B) Arrangement of FlgE subunits in the hook. Major helical lines are indicated by arrows. The FlgE subunits along the 11-start helical line comprise the protofilament. The number labeled on the subunits represents the number of the subunit starting from the central subunit (subunit 0) along the 1-start helical line. The number also shows the direction of the helical line. FlgE monomers are sequentially assembled along the 1-start helix.

assembles directly on the FliE zone, followed by FlgC and, finally, FlgF. The FlgB subunits also interact with the inner wall of the MS ring, stabilizing the interaction between the MS ring and the proximal rod. Genetic analyses have

revealed that the FliE zone is stabilized by intermolecular interactions between FliE, FlgB, and FlgC (75, 76). As a result, the proximal rod binds strongly to both the FliP₅-FliR₁ complex and the MS ring and does not detach from the MS ring even when the flagellar motor generates high torque or rotates at high speed. FlgG consists of three domains, D0, Dc, and D1, and domains D0 and D1 of FlgG are both highly packed in all three main helical directions, the left-handed 5-start, the right-handed 6-start, and the 11-start helices, in each of the inner and outer radial regions of the rod (Fig. 8A) (77). A β -hairpin structure of domain Dc named the L stretch straightens and stiffens the rod, allowing the rod to act as a driveshaft of the flagellar motor (78).

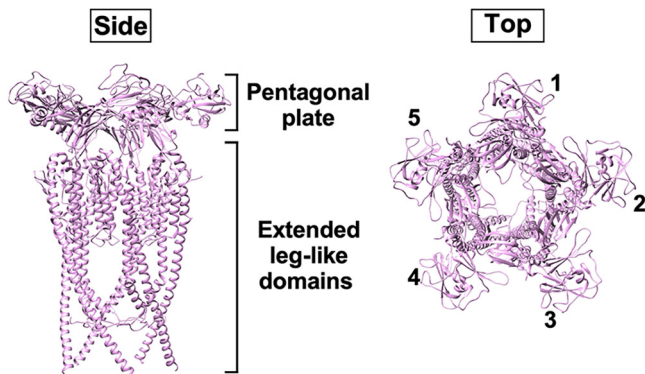


FIG 6 CryoEM structure of the filament cap. Shown are side (left) and top (right) views of the atomic model of the filament cap in C_α ribbon representation (PDB accession number 6SIH). Five FliD subunits self-assemble into the filament cap structure consisting of a pentagonal plate and five extended leg-like domains.

(ii) Hook. The hook is a short, highly curved tubular structure. The hook is flexible with respect to bending but is rigid against twisting. In *Salmonella*, the bending flexibility of the hook allows several flagellar filaments

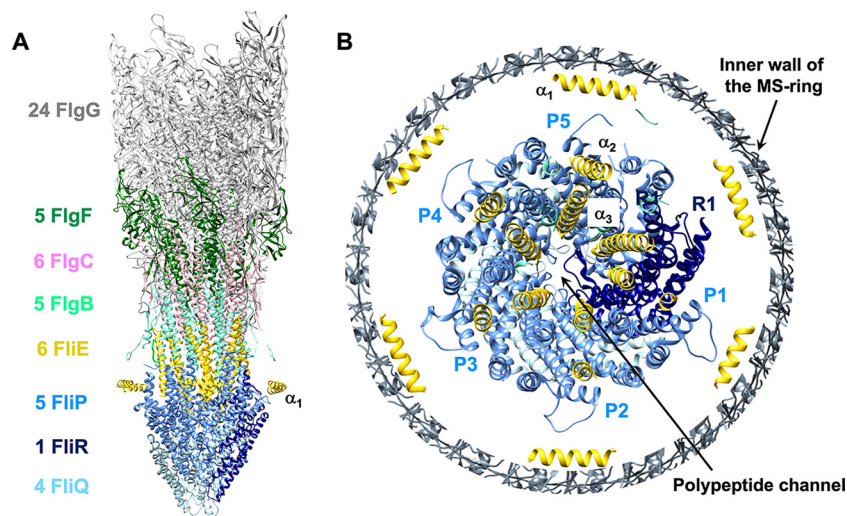


FIG 7 CryoEM structure of the rod. (A) Atomic model of the rod in C_{α} ribbon representation (PDB accession number 7CGO). The rod consists of 6 FliE (gold), 5 FlgB (aquamarine), 6 FlgC (pink), 5 FlgF (dark green), and 24 FlgG (light gray) subunits and is connected directly to the polypeptide channel complex consisting of 5 FliP subunits (cornflower blue), 4 FliQ subunits (light blue), and 1 FliR subunit (navy blue). (B) Interactions of FliE with the MS ring, FliP, and FliR. FliE consists of three α -helices, α_1 , α_2 , and α_3 . Helix α_1 binds to the inner wall of the MS ring. Helices α_2 and α_3 of FliE, which form domain D0, bind to either the FliP or the FliR subunit of the polypeptide channel complex to form the most proximal part of the rod inside the MS ring. Helix α_2 is invisible when FliE binds to FliR.

to form a bundle behind the cell body, pushing the cell forward (79). The hook is composed of about 120 FlgE subunits, so the length of the hook is fairly well defined (about 55 nm in *Salmonella*) (80). The hook length control mechanism is described below. FlgE is composed of four domains, D0, Dc, D1, and D2, that are arranged from the inner to the outer parts of the hook structure (Fig. 8B) (81, 82). Extensive interactions between the D0 domains of FlgE not only are important for hook assembly but also structurally and mechanically stabilize the hook structure. Interestingly, gaps between D0 domains are also observed at key points, allowing enough space for the hook structure to exert bending flexibility. Domains Dc and D1 are also involved in hook assembly with the help of the hook cap formed by FlgD (83, 84). Domain D2 is dispensable not only for hook assembly but also for the universal joint function (85).

The D0, Dc, and D1 domains of FlgE are nearly identical in conformation to the D0, Dc, and D1 domains of FlgG, respectively, and hence, FlgE can assemble directly onto the tip of the distal rod (77, 78). However, the L stretch of domain Dc of FlgE is 18 amino acid residues shorter than that of FlgG. When the extra 18

residues of FlgG are inserted into the Dc domain of FlgE, the hook becomes rigid and straight (86). The L stretch of FlgG extensively contacts the D1 domains of other FlgG subunits in the distal rod structure, providing stability and stiffness to the rod (Fig. 8A) (78). However, the interaction between FlgE subunits via the L stretch of FlgE is not as extensive as that seen in the rod, so gaps are also observed between the D1 domains of FlgE in the hook structure (Fig. 8B) (87). Therefore, these gaps between the D1 domains seem likely to give the hook bending flexibility and allow the hook to undergo sequential compression-and-extension cycles along the tubular axis during flagellar motor rotation.

The hook undergoes polymorphic transformations of its supercoiled form in response to the salt concentration, pH, and temperature of the solution (88). Domain D2 of FlgE is the outermost part of the hook structure (Fig. 8B). In each protofilament, domain D2 of the lower FlgE subunit interacts with a triangular loop of domain D1 of the upper FlgE subunit (D1 loop) (81). Because the deletion of either domain D2 or the D1 loop from FlgE makes the hook straight but allows it to retain its bending flexibility, the direction of intermolecular D2-D2 interactions along

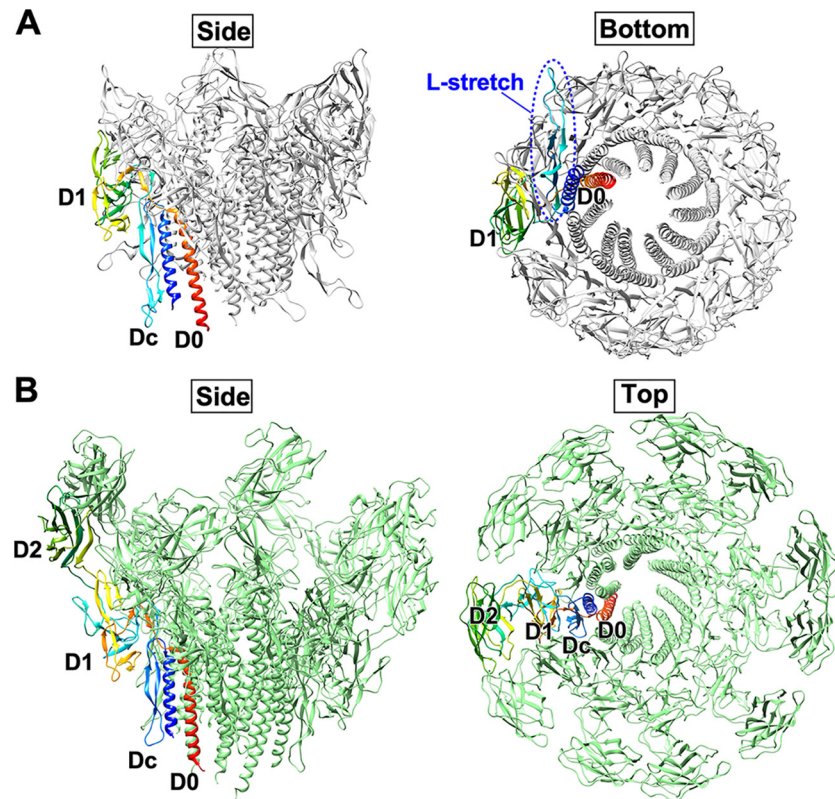


FIG 8 Structural comparison of the distal rod and hook. (A) Atomic model of the distal rod in C_{α} ribbon representation (PDB accession number 7CGO). FlgG is composed of three domains, D0, Dc, and D1, that are arranged from the inner to the outer parts of the distal rod. The L stretch of domain Dc of FlgG makes the rod straight and rigid. (B) Atomic model of the native supercoiled hook in C_{α} ribbon representation (PDB accession number 7CGO). FlgE is composed of four domains, D0, Dc, D1, and D2, that are arranged from the inner to the outer parts of the hook. Gaps between FlgE subunits are responsible for the bending flexibility of the hook structure.

each protofilament of the hook structure influences the curvature and twist of each supercoil (85). Recent high-resolution cryoEM image analyses of the native supercoiled hook structure have shown that the conformation of the FlgE subunit gradually changes along the circumference from one protofilament to the next. The conformations of subunits are nearly identical within each protofilament, and hence, there are 11 distinct conformations. Thus, changes in the positions and orientations of domains D1 and D2 of FlgE relative to domain D0 appear to be important for the supercoiling of the hook (89, 90). Because domain Dc of FlgE plays a critical role in the polymorphic transformations of the supercoiled hook, domain Dc would be equipped with a structural switch that alters the relative domain position and orientation of FlgE during the compression-and-extension cycle of each protofilament (84, 86).

(iii) Filament. The flagellar filament grows up to $15\ \mu\text{m}$ in length by the assembly of about 30,000 flagellin molecules. Flagellin consists of four domains, D0, D1, D2, and D3, arranged from the inner core to the outer surface of the filament (91). Domains D0 and D1 are well conserved among flagellin homologs, whereas domains D2 and D3 are not (92), suggesting that the D0 and D1 domains are critical not only for filament formation but also for molecular function as the helical propeller.

The filament is a supercoiled structure and undergoes polymorphic transformations of its supercoiled form during motility. The left-handed supercoil of the filament is called a “normal” filament. When each motor spins in the CCW direction, several normal filaments form a bundle structure behind the cell body, and this bundle rotates like a screw to propel the cell body. A quick reversal of the motor

to CW rotation generates torsional force, which converts the normal filament to right-handed helical forms called either “semicoiled” or “curly.” As a result, the bundle structure is disrupted, so the cell tumbles and changes swimming direction (93). Thus, the polymorphic transformation of the filament is very important for efficient flagellum-driven motility.

Domains D0 and D1 of FliC are important for the polymorphic transformation of *Salmonella* flagellar filaments, and a β -hairpin in the D1 domain has been postulated to act as a structural switch that changes the left-handed and right-handed helical forms of the filament (94). The G426A and A449V mutations in domain D1 of FliC give rise to L- and R-type straight filaments, respectively (95). Purified L- and R-type FliC subunits self-assemble into L- and R-type straight filaments, respectively, *in vitro*. On the other hand, when filaments are polymerized by mixing purified L- and R-type FliC subunits, the reconstituted filaments take on various helical shapes depending on the ratio of the two types of FliC subunits (96, 97). Thus, the polymorphic transformation of the filament can be well explained by a bistable protofilament model in which supercoiled forms can be produced by combinations of two distinct conformations and packing interactions of L- and R-type protofilaments (98–101). CryoEM image analyses of L- and R-type straight filaments have shown that the conformation of the lower part of domain D0 of FliC differs between the L- and R-type filament structures, resulting in a hinge motion of the remaining three domains relative to domain D0, with a hinge at the spoke region connecting domains D0 and D1 (91, 102). Thus, the hinge motion between domains D0 and D1 seems to be responsible for the switching between L-type and R-type protofilaments. Recently, normal and curly I filaments have been analyzed by cryoEM image analysis, which revealed that there are 11 different protofilament states in these two filament structures in a way similar to that of the supercoiled hook. The interfaces between different protofilaments cluster into distinct groups, allowing the allosteric switching of the filament (103). Thus, these two cryoEM structures may overturn the long-standing model of the supercoiling mechanism of the filament structure.

Domain D3 of flagellin is recognized as an H antigen by the host immune system. *Salmonella* possesses two distinct flagellin genes, namely, *fliC* and *fljB*, at distinct locations in the *Salmonella* genome. Because the primary sequence of domain D3 of FliC is very different from that of FljB, FliC

and FljB are named H1 and H2 antigens, respectively. Because only one of these two flagellin genes is expressed at any given time, each *Salmonella* cell produces homologous filaments. This alternative expression stochastically occurs at a frequency of 10^{-3} to 10^{-5} per cell per generation. This phenomenon is called flagellin phase variation. Because the phase variation results in the appearance of two *Salmonella* species with completely different flagellar antigens (104), it is thought to be a mechanism for escaping the host immune system by altering flagellar antigenicity. Recently, a high-resolution cryoEM image analysis of the FljB filament showed that domain D3 of FljB is more flexible and mobile than that of FliC (105). Because the swimming behavior of *Salmonella* cells producing the FljB filaments is different from that of the cells producing the FliC filaments under high-viscosity conditions (106), such structural differences in the D3 domains of FliC and FljB are likely to be functional differences between these two filaments. Thus, flagellin phase variation also plays an important role in optimizing the mechanical function of the filament as a helical propeller under different conditions.

Surface-exposed lysine residues of both FliC and FljB are methylated by a flagellum-specific methylase named FliB. Loss-of-function mutations in the *fliB* gene do not affect *Salmonella* motility, indicating that FliB is dispensable for flagellum-driven locomotion (107–109). Because the methylation of the flagellin subunit by FliB significantly increases the hydrophobicity of the outer surface of the filament, *Salmonella* cells efficiently adhere to the hydrophobic host cell surfaces, thereby increasing the probability of host cell invasion (110). Thus, the filament also plays an important role in the infection processes involving bacterial adhesion.

(iv) Hook-filament junction. The hook-filament junction structure is composed of 11 FlgK (HAP1) subunits and 11 FlgL (HAP3) subunits and is located between the hook and the filament. Because the atomic structures of FlgE and FliC are in different conformations (81, 94), the filament cannot grow directly from the tip of the hook. So if the hook-filament junction structure is missing, the newly exported flagellin molecules simply leak out into the culture medium (111, 112). Because the hook is flexible against bending, whereas the filament is rigid, the hook-filament junction structure serves as a buffering structure connecting the hook and the filament with distinct mechanical properties

(113). This is supported by the crystal structures of FlgK and FlgL (114, 115).

(v) Cap structures. The flagellar axial structure grows at its distal end. Distal growth has been directly observed in experiments with filaments both *in vivo* and *in vitro* (116–119). Purified FlgE and FliC monomers can self-assemble into hooks and filaments, respectively, under *in vitro* conditions (116, 118). *In vivo*, on the other hand, FlgJ, FlgD, and FliD (HAP2) are required for the efficient assembly of the rod, hook, and filament structures, respectively (120–122).

FliD self-assembles into a homopentamer at the tip of the hook-filament junction structure, and this FliD pentamer acts as the filament cap to support the assembly of newly transported flagellin subunits into the filament at the growing end of the filament (112, 122, 123). If the filament cap is missing, large amounts of flagellin leak into the culture medium in a monomeric form (111). Thus, the filament cap appears to suppress the leakage of newly transported flagellin monomers into the culture medium, thereby allowing unfolded flagellin molecules to have enough time to refold and assemble into the filament. FliD consists of domains D0, D1, D2, and D3. The filament cap is divided into two structural parts: a pentagonal plate as a lid and five axially extended leg-like domains that bind to the filament at the distal end (Fig. 6). Domains D0 and D1 form the leg-like domain, whereas domains D2 and D3 form part of the pentagonal plate. The filament cap provides a large cavity under the pentagonal plate as a folding chamber for the newly exported flagellin molecules in the unfolded conformation to be folded and incorporated into an appropriate assembly position at the distal end of the filament (123–126).

The hook cap consists of 5 copies of FlgD and exists at the hook tip to promote the assembly of FlgE monomers into the hook structure (127). FlgD is composed of a flexible N-terminal region (FlgD_N) directly involved in the hook polymerization process and a compactly folded domain (FlgD_C) that prevents newly exported FlgE molecules from leaking out into the culture medium (83). Five FlgD_N subunits form an α -helical bundle as a central stalk, whereas five FlgD_C subunits form a petal-shaped head (22, 127). Unlike the filament cap, the hook cap does not have a folding chamber beneath the petal-shaped head because the central stalk is

inserted deeply into the central channel of the growing hook structure. Instead, the hook cap provides a space around the stalk, allowing the newly transported FlgE molecules in the unfolded conformation to be efficiently folded and incorporated into the hook structure (127). When hook assembly is finished, the hook cap is removed from the hook tip by the first hook-filament junction protein FlgK (121). Thus, the hook cap is not part of the mature flagellum.

The hook and filament structures have helical symmetry, whereas the hook and filament caps have 5-fold rotational symmetry. Due to this symmetry mismatch between the cap structure and the helical tubular structure, it has been proposed that each time that a structural subunit is exported, folded, and incorporated into the helical structure, the cap rotates and moves up along the helical structure, thereby creating the next assembly point (123, 127).

The diameter of the distal rod is 13 nm (77), and at this diameter, the distal rod cannot penetrate the PG layer. FlgJ is thought to act as the rod cap to facilitate rod assembly in a way similar to that of FlgD and FliD. FlgJ is composed of an N-terminal domain directly involved in rod assembly and a C-terminal domain acting as a flagellum-specific muramidase that hydrolyzes the PG layer (120). A loss of the PG-hydrolyzing activity of FlgJ results in extremely poor flagellar formation, suggesting that the muramidase activity of FlgJ working at the tip of the growing rod structure is important for the distal rod to efficiently penetrate the PG layer (128). Because the L-ring assembly around the distal rod induces the dissociation of the rod cap from the rod tip (129), the rod cap is not part of the mature flagellum.

Structure and function of the flagellar type III secretion system. The protein export apparatus of the flagellum is very similar in structure and function to that of the injectisome of pathogenic bacteria, which directly injects virulence effector proteins into host cells for invasion, so both are classified as type III secretion systems (130). The flagellar type III secretion system (fT3SS) is located at the base of the flagellum and transports flagellar axial proteins from the cytoplasm at a rate of up to tens of thousands of amino acids per second to construct the flagellar axial structure beyond the cytoplasmic membrane (119, 131). The fT3SS is composed of a cytoplasmic ATPase ring complex with a stoichiometry of 12 FliH subunits, 6 FliI

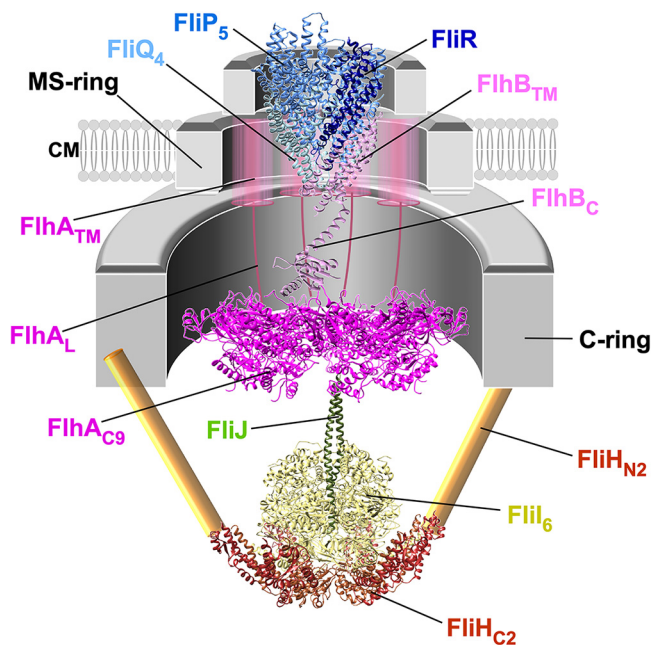


FIG 9 Structure of the FT3SS. Shown are atomic models of the FlhB₁-FliP₅-FliQ₄-FliR₁ complex (PDB accession number 6S3L), the C-terminal cytoplasmic domain of FlhB (FlhB_C) (PDB accession number 3B0Z), the C-terminal cytoplasmic domain of FlhA (FlhA_C) (PDB accession number 3A5I), the FliH_{C2}-FliI complex (PDB accession number 5B00), and FliJ (PDB accession number 3AJW) in C_α ribbon representation. There is no atomic model for the N-terminal transmembrane domain of FlhA with eight transmembrane helices (FlhA_{TM}) and the N-terminal domain of FliH (FliH_N). Because the electron density corresponding to FlhB_C in the cryoEM structure of the FlhB₁-FliP₅-FliQ₄-FliR₁ complex is very poor, the position of FlhB_C relative to FlhB_{TM} remains unknown. The flagellar type III secretion system consists of a transmembrane export gate complex with a stoichiometry of 9 FlhA subunits (magenta), 1 FlhB subunit (plum), 5 FliP subunits (cornflower blue), 4 FliQ subunits (light blue), and 1 FliR subunit (navy blue) and a cytoplasmic ATPase ring complex with a stoichiometry of 12 FliH subunits (brown), 6 FliI subunits (khaki), and 1 FliJ subunit (dark olive green). The transmembrane export gate complex is located within the MS ring. FliJ binds to the center of the FliI₆ ring, and two C-terminal domains of the FliH dimer (FliH_{C2}) bind to different regions of the N-terminal domain of each FliI subunit of the FliI₆ ring. The FliI₆-FliJ ring complex is tightly bound to the C ring by the interaction between FliH_{N2} and FliN in the C ring. CM, cytoplasmic membrane.

subunits, and 1 FliJ subunit and a transmembrane export gate complex with a stoichiometry of 9 FlhA subunits, 1 FlhB subunit, 5 FliP subunits, 4 FliQ subunits, and 1 FliR subunit (Fig. 9) (132–134).

(i) Cytoplasmic ATP complex. FliI, a flagellum-specific ATPase, self-assembles into a homo-hexamer (135, 136).

FliJ adopts an antiparallel coiled coil and binds to the center of the FliI₆ ring (137). The overall structure of the FliI₆-FliJ₁ ring complex is very similar to that of the $\alpha_3\beta_3\gamma$ ring complex of the F₀F₁ ATP synthase, the minimum unit that can act as an ATP-driven rotary motor to couple ATP hydrolysis by the β -subunit with the rotation of the γ -subunit within the $\alpha_3\beta_3$ ring (137, 138). FliH forms a homodimer via a central α -helical coiled coil (139), and the FliH dimer is structurally and functionally similar to the peripheral stalk of the F₀F₁ ATP synthase that connects F₀ and F₁ (140, 141). Two C-terminal domains of the FliH dimer bind with high affinity to different regions of the N-terminal domain of each of the six FliI subunits (141). The extreme N-terminal region of FliH binds to FliN in the C ring, thereby anchoring the FliI₆-FliJ₁ ring complex to the base of the flagellum (Fig. 9) (142). The FliH₁₂-FliI₆-FliJ₁ ring complex is thought to act as an activator of the transmembrane export gate complex, so ATP hydrolysis by the FliI₆ ring has been postulated to transform the inactive export gate complex into a highly efficient protein transporter through the interaction of FliJ with the C-terminal cytoplasmic region of FlhA (143, 144).

In addition, the FliH dimer and the FliI ATPase are present in the cytoplasm as the heterotrimeric FliH₂-FliI₁ complex (145). The FliH₂-FliI₁ complex also localizes to the flagellar base via interactions of FliH with FliN in the C ring and FlhA in the export gate complex (146, 147). High-resolution single-molecule imaging techniques have shown that the FliH₂-FliI₁ complex shows rapid exchanges between the basal body and a freely diffusing cytoplasmic pool in an ATP-independent manner (148). Furthermore, *in vitro* protein transport assays have revealed that the addition of the purified FliH₂-FliI₁ complex considerably enhances flagellar protein export by the export gate complex in a protein-concentration-dependent manner (149, 150). Because the FliH₂-FliI₁ complex binds to export substrates and chaperone-substrate complexes (151, 152), this complex has been proposed to serve as a dynamic carrier that efficiently and rapidly delivers them to the export gate complex.

(ii) Transmembrane export gate complex. When the cytoplasmic ATPase complex is fully functional in the FT3SS, the transmembrane export gate complex uses PMF as the primary energy source and functions as an H⁺/protein antiporter that couples inward-directed H⁺ flow with outward-directed protein translocation (153–155). However,

when the cytoplasmic ATPase complex is absent or non-functional, the export gate complex itself prefers to use sodium motive force across the cytoplasmic membrane and serves as a Na^+ /protein antiporter over a wide range of external pHs (156, 157). Furthermore, when the electric potential difference ($\Delta\Psi$) across the cell membrane, which is defined as membrane voltage, exceeds a certain threshold value, an inactive export gate complex autonomously becomes an active H^+ /protein antiporter to a considerable degree (158). Thus, the export gate complex has a polypeptide channel, a dual-fuel protein export engine that uses either H^+ or Na^+ as the coupling ion to drive cation-coupled protein export, a membrane voltage sensor, and a substrate-docking platform.

FliP, FliQ, and FliR form the polypeptide channel complex with a stoichiometry of 5 FliP subunits, 4 FliQ subunits, and 1 FliR subunit, allowing export substrates to be translocated across the cytoplasmic membrane (159). The FliP₅-FliQ₄-FliR₁ complex is formed by the helical arrangement of subunits within a central pore of the MS ring (Fig. 9). The exit gate of the polypeptide channel of the purified FliP₅-FliQ₄-FliR₁ complex is closed, but the exit gate of the polypeptide channel of the FliP₅-FliQ₄-FliR₁ complex in the native basal body is open. Because six FliE subunits assemble directly on FliP or FliR (Fig. 7B) (22, 23), interactions of FliE with FliP and FliR induce helical rearrangements of the polypeptide channel, resulting in the open conformation of the exit gate. A single copy of FlhB binds to the FliP₅-FliQ₄-FliR₁ complex via interactions of the N-terminal transmembrane domain of FlhB (FlhB_{TM}) (residues 1 to 211) with FliP, FliQ, and FliR (Fig. 9), and a cytoplasmic loop between TMH-2 and TMH-3 of FlhB_{TM} firmly associates with the entrance gate of the FliP₅-FliQ₄-FliR₁ complex (160). Genetic and biochemical analyses have suggested that the C-terminal cytoplasmic domain of FlhB (FlhB_C) (residues 212 to 383) regulates the opening and closing of this entrance gate along with the cytoplasmic ATPase complex (161). Because FlhB_C provides binding sites for export substrates (162, 163), the binding of export substrates to FlhB_C seems to open the entrance gate of the polypeptide channel.

Nine FlhA subunits assemble around the FlhB₁-FliP₅-FliQ₄-FliR₁ complex via intermolecular interactions between the C-terminal cytoplasmic domains (FlhA_C) (residues 362 to 692) (164). The homonameric ring structure of FlhA_C (FlhA_{C9}) projects into the central cavity of the C ring (Fig. 9)

(165) and functions as a docking platform for components of the cytoplasmic ATPase complex, flagellar export chaperones, and export substrates (166–170). FlhA shows both H^+ and Na^+ channel activities, suggesting that the N-terminal transmembrane domain of FlhA (FlhA_{TM}) (residues 1 to 327) presumably functions as a dual-fuel protein export engine (156). FliJ binds with high affinity to the flexible linker region of FlhA (FlhA_L) (residues 328 to 361) connecting FlhA_{TM} and FlhA_C and with low affinity to FlhA_C, not only activating the H^+ channel activity of FlhA_{TM} but also unlocking the entrance gate of the polypeptide channel (143, 171). Because the FliJ-FlhA interaction is significantly stabilized by an increase in $\Delta\Psi$, FlhA seems to be equipped with a voltage-gated mechanism (158).

(iii) Substrate-specific export chaperones. In the cytoplasm, flagellar export chaperones are required to efficiently transport flagellar structural subunits that form the hook-filament junction (FlgK and FlgL), the filament (flagellin), and the filament cap (FliD). Three flagellar proteins are known as substrate-specific export chaperones: FlgN for FlgK/FlgL, FliS for flagellin (FliC or FliJ), and FliT for FliD (172, 173). Each flagellar chaperone binds to the C-terminal disordered region of its export substrate and suppresses the premature aggregation and proteolysis of the substrate in the cytoplasm (174, 175). The FlgN, FliS, and FliT chaperones adopt an α -helical structure (141, 176, 177). When the export substrate binds to its cognate chaperone, a helical rearrangement of the chaperone structure occurs, allowing the chaperone-substrate complex to bind with high affinity to FlhA_C (178, 179). The chaperone-FlhA_C interaction allows the transmembrane export gate complex to efficiently unfold and transport the substrates (180, 181). FlhA_C undergoes cyclic open-closed domain motions during flagellar protein export (182). The chaperone-substrate complex can bind to the open form of FlhA_C but not the closed form (183, 184), leading to the plausible hypothesis that the conformational change from the open to the closed conformations of the FlhA_C subunit in the FlhA_{C9} ring would trigger the dissociation of the empty chaperone from this FlhA_C subunit for the binding of the newly delivered chaperone-substrate complex.

Structure and function of the force generator. (i) Transmembrane MotA₅-MotB₂ complex. The *Salmonella* flagellar motor is powered by PMF across the cytoplasmic membrane. MotA and MotB form a transmembrane

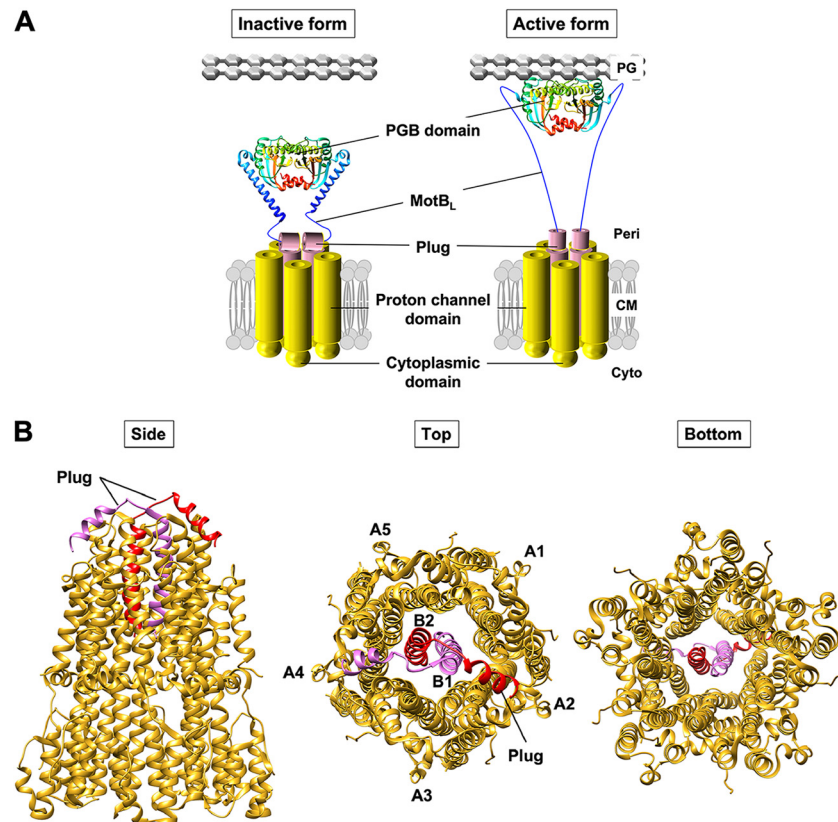


FIG 10 Structure of the MotA₅-MotB₂ complex. (A) Model for the inactive and active forms of the MotA₅-MotB₂ complex. The MotA₅-MotB₂ complex is divided into four distinct functional parts: a cytoplasmic domain responsible for the interaction with the rotor protein FliG, a transmembrane proton (H⁺) channel domain involved in inward-directed H⁺ flow, a peptidoglycan (PG)-binding domain (PGB) responsible for binding to the PG layer (PDB accession number [2ZVY](#)), and a flexible linker region containing a plug helix. (Left) When the PGB domain adopts a compact conformation, the plug helix binds to the H⁺ channel domain to suppress massive H⁺ flow. (Right) When the inactive MotA₅-MotB₂ complex, which is freely diffusing across the cytoplasmic membrane, encounters a rotor, interactions between its cytoplasmic domain and FliG are postulated to trigger the dissociation of the plug segment from the H⁺ channel, followed by the unfolding of the N-terminal α -helix of the PGB domain, which extends 5 nm and binds the PG layer. As a result, the MotA₅-MotB₂ complex becomes a force generator to drive flagellar motor rotation. PG, peptidoglycan layer; Peri, periplasmic space; CM, cytoplasmic membrane; Cyto, cytoplasm. (B) CryoEM structure of the MotA₅-MotB₂ complex. Shown is an atomic model of the purified MotA₅-MotB₂ complex in C α ribbon representation (PDB accession number [6YKM](#)). The five MotA subunits (goldenrod) form a pentameric ring structure, with two transmembrane helices of the MotB dimer (red and orchid) bound to the center of the MotA ring. Each plug helix of the MotB dimer binds to the periplasmic loop of MotA.

H⁺ channel complex in the cytoplasmic membrane, and the MotA-MotB complex acts as a force generator for the flagellar motor that couples inward-directed H⁺ flow through the H⁺ channel with torque generation. The MotA-MotB complex is divided into four distinct parts: a cytoplasmic domain responsible for the interaction

with the rotor protein FliG, a transmembrane H⁺ channel domain involved in H⁺ transfer from the periplasm to the cytoplasm, a peptidoglycan-binding (PGB) domain responsible for the interaction with the PG layer, and a flexible linker region connecting the H⁺ channel domain and the PGB domain (Fig. 10A) ([9](#), [10](#), [15](#), [185](#)).

MotA has four TMHs, TMH-1, TMH2, TMH-3, and TMH-4; two short periplasmic loops between TMH-1 and TMH-2 and between TMH-3 and TMH-4; a cytoplasmic domain (MotA_C) between TMH-2 and TMH-3; and a C-terminal cytoplasmic tail (186). MotB is composed of a short N-terminal cytoplasmic tail, a single TMH, a flexible linker region (MotB_L), and a PGB domain (187). Each MotB TMH forms an H⁺ translocation pathway with TMH-3 and TMH-4 of MotA, so the MotA-MotB complex has two distinct H⁺ translocation pathways (188, 189). Two residues that are well conserved in the H⁺ translocation pathway, Asp33 in MotB and Pro173 in MotA, are both directly involved in H⁺ translocation that is coupled with torque generation (190–193). MotA_C contains the highly conserved residues Arg90 and Glu98 that are responsible for the interaction with FliG (42). The PGB domain of MotB forms a dimer, and its dimerization is important for the force generators placed around the rotor to be firmly anchored to the PG layer (194). MotA and MotB had been believed to form a heterohexamers with a stoichiometry of 4 MotA and 2 MotB subunits (195). However, recent high-resolution cryoEM image analyses have revealed that the MotA-MotB complex is composed of five MotA subunits and two MotB subunits (Fig. 10B). The five MotA subunits form a pentameric ring (MotA₅), and two TMHs of MotB penetrate the central pore of the MotA₅ ring. Based on the cryoEM structure of the MotA₅-MotB₂ complex, a torque generation mechanism model has been proposed in which the MotA₅ ring rotates around the TMHs of the MotB dimer in response to H⁺ transfer through the H⁺ channel, turning the rotor like a small gear turning a large gear (196, 197).

MotB_L (residues 51 to 100) is dispensable for flagellar motor rotation (198). Residues 53 to 66 of MotB_L adopt a short α -helix and bind to the periplasmic loop between TMH-3 and TMH-4 of MotA (Fig. 10B) (196). This short α -helix acts as a plug that blocks the flow of H⁺ through the H⁺ channel until the MotA₅-MotB₂ complex assembles around the rotor of the flagellar motor and functions as a force generator (199, 200). Thus, MotB_L coordinates H⁺ translocation through the channel with torque generation by MotA_C-FliG interactions.

The N-terminal portion of the PGB domain of MotB takes on two distinct conformations: a compact conformation and an extended conformation (Fig. 10A). For the MotA₅-MotB₂ complex to become a force generator in the flagellar motor, the PGB domain must extend 5 nm from the transmembrane H⁺ channel domain to

bind to the PG layer (194, 201). The 5-nm extension process of the PGB domain of MotS from *Bacillus subtilis*, a MotB homolog, has been directly visualized by high-speed atomic force microscopy. The 5-nm extension of the PGB domain occurs in at least two steps. The first 2.5-nm extension occurs when the plug helix is detached from the H⁺ channel domain, and the next 2.5-nm extension is triggered by an order-to-disorder transition of the N-terminal portion of the PGB domain (202). The MotB(L119P) substitution located in the N-terminal portion of the PGB domain induces a conformation change in the N-terminal portion of the PGB domain, which not only activates the H⁺ channel activity of the MotA₅-MotB₂ complex but also allows the PGB domain to bind with high affinity to the PG layer (201). This suggests that MotB_L also regulates not only the proper H⁺ channel formation of the MotA₅-MotB₂ complex but also the efficient and proper anchoring of the PGB domain to the PG layer.

(ii) Load-dependent stator assembly. Each MotA₅-MotB₂ complex binds to and dissociates from a rotor during flagellar motor rotation, suggesting that the force generator is a highly dynamic structure (203). The number of force generators in the motor changes as the external load changes. When the flagellar motor operates at high loads, the number of force generators placed around the rotor is about 10 (Fig. 11, left). On the other hand, when the external load is very low, the number of force generators decreases from 10 to a few (Fig. 11, right). Thus, the flagellar motor autonomously controls the number of force generators placed around the rotor in response to changes in the external load (204, 205). An in-frame deletion of residues 72 to 100 of MotB_L results in a very steep decrease in the number of force generators with decreasing external loads compared to the wild-type motor (206). This suggests that MotB_L regulates the binding affinity of the PGB domain for the PG layer in a load-dependent manner. Certain point mutations in MotA_C, which is involved in the interaction with FliG, change the load sensitivity of the MotA₅-MotB₂ complex (207), suggesting that MotA_C is equipped with a load sensor that adjusts the number of force generators placed around the rotor in response to changes in the external load.

FLAGELLAR GENE REGULATION

Control of gene expression. Many flagellar and related genes are organized into at least 17 operons in the

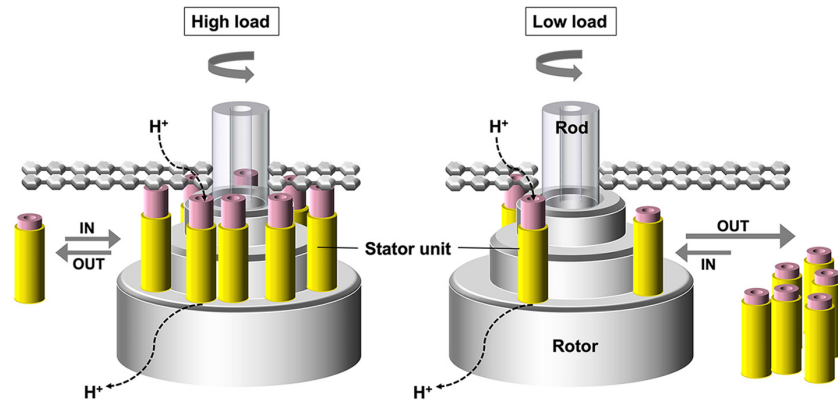


FIG 11 Load-dependent stator assembly mechanism. (Right) At very low loads, a few stator units surround the rotor. (Left) As the external load increases, the number of active stator units increases to a maximum of about 10. The association rates of the stator unit are essentially the same for both low and high loads, but the dissociation rate is much higher at low loads than at high loads.

Salmonella genome. These genes are not expressed constitutively but rather are expressed in a temporal hierarchy that reflects the process of flagellar assembly. The flagellar operons are organized into a transcriptional

hierarchy of three promoter classes, classes 1, 2, and 3, based on how they are temporally expressed (Fig. 12) (208). At the top of the hierarchy is the *flhDC* operon, which contains two genes, *flhD* and *flhC*, in that order. The class 1 promoter is

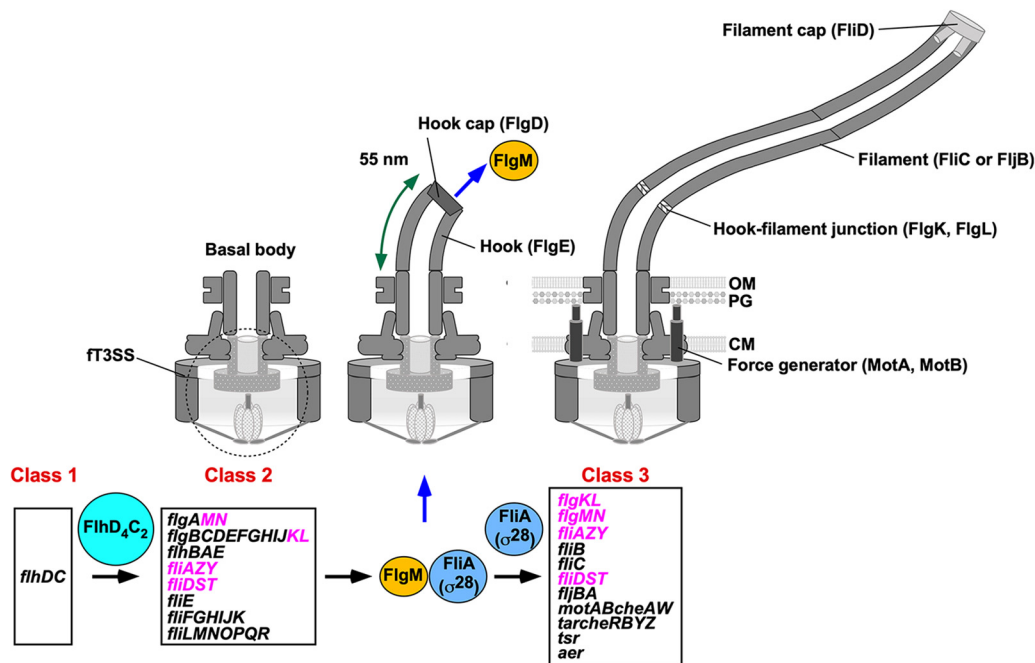


FIG 12 Hierarchical flagellar gene expression in *Salmonella*. Flagellar assembly begins with the basal body, followed by the hook and, finally, the filament. FlhD and FlhC form the FlhD₄-FlhC₂ complex that induces transcription from class 2 promoters, thereby producing several hook-basal bodies (HBBs) on the *Salmonella* cell surface. During HBB assembly, FlgM binds to FliA to inhibit transcription from class 3 promoters. When the hook length reaches its mature length of 55 nm, FlgM is secreted via the σ^{28} into the culture medium. As a result, FliA can act as a flagellum-specific sigma factor (σ^{28}), allowing RNA polymerase to transcribe class 3 genes encoding proteins required for filament formation, motility, and chemotaxis. The *flgKL*, *flgMN*, *flhAZY*, and *flhDST* operons highlighted in magenta are transcribed from both class 2 and class 3 promoters. OM, outer membrane; PG, peptidoglycan layer; CM, cytoplasmic membrane.

under the control of several global regulators that determine when the *flhD* and *flhC* genes are transcribed in response to various signals in the cell (209). Because these two genes are absolutely required for the expression of all other genes in the flagellar regulon, the *flhDC* operon is called the master operon. FlhD and FlhC form the FlhD₄-FlhC₂ complex that allows RNA polymerase containing σ^{70} to bind to class 2 promoters. The class 2 genes encode proteins required for the structure and assembly of the hook-basal body (HBB). Two transcriptional regulator genes, *fliA* and *flgM*, are present at the class 2 level. FliA is a flagellum-specific sigma factor (σ^{28}) that induces the transcription of class 3 genes encoding proteins required for filament formation, motility, and chemotaxis (210). FlgM binds directly to FliA and inhibits the σ^{28} activity of FliA until the hook structure is completed. Thus, FlgM acts as an anti-sigma factor during HBB assembly (211). Once hook formation is complete, FlgM is secreted via the σ^{28} into the culture medium, allowing FliA to become an active σ^{28} that induces transcription from class 3 promoters (212, 213). In HBB formation-defective mutants, FlgM remains in the cytoplasm, so class 3 genes are not transcribed. Thus, the σ^{28} seems to serve as a transcriptional regulator that couples flagellar gene expression with assembly.

Four flagellar operons, namely, the *flgKL*, *flgMN*, *fliAZY*, and *fliDST* operons, are expressed from both class 2 and class 3 promoters (Fig. 12). The *fliAZY* and *fliDST* operons possess two distinct class 2 and class 3 promoters. On the other hand, since the *flgKL* and *flgMN* operons do not have their own class 2 promoters, the FliA-independent transcription of the *flgKL* and *flgMN* operons is likely the result of readthrough from their upstream operons (214–216). The expression of FlgK, FlgL, and FliD from their class 3 promoters has been shown to be critical for flagellum-driven motility under high-viscosity conditions (217). Because FlgN, FliT, FliS, and FliZ are known as regulators involved in flagellar gene expression (218–222), these multiple flagellar promoters can efficiently respond to changing environmental conditions and coordinate flagellar gene expression with assembly. As a result, the flagellum-driven motility of *Salmonella* is optimized under a variety of environmental conditions.

Control of flagellin phase variation. As mentioned above, *Salmonella* has two distinct flagellin genes, *fliC* and *fliB*, and their expression is stochastically controlled at a frequency of 10^{-3} to 10^{-5} per cell per generation, allowing

Salmonella cells to possess either FliC or FliB filaments. This alternative flagellin expression pattern mechanism is under the control of a DNA invertase called Hin that promotes site-specific DNA recombination (223). Because the *fliB* gene forms an operon together with the *fliA* gene, whose gene product inhibits the translation of FliC (224), the expression of the *fliC* gene is suppressed in cells in which the *fliBA* operon is expressed. On the other hand, the *fliBA* operon is not expressed in cells in which FliC is expressed. Such an alternative expression pattern of the *fliBA* operon is mediated by the inversion of a reversible 970-bp region of DNA upstream of the *fliB* gene (*hin* region) that contains the class 3 promoter of the *fliBA* operon (223). In one orientation, the promoter is in the proper position and orientation for the initiation of the transcription of the *fliBA* operon, while in the other, it is not. The reversible *hin* region is sandwiched between two inverted repeat sequences, namely, *hixL* and *hixR*, which allow the Hin invertase to invert the *hin* region by homologous recombination. During inversion, the Hin invertase assembles with two histone-like proteins, Fis and HU, each of which binds to the enhancer sequence within the *hin* region, into a multicomponent complex called the invertosome. As a result, the Hin invertase can efficiently catalyze the flipping of this *hin* region (225, 226).

The *hin* region contains the *hin* gene and its promoter, so the Hin invertase can be expressed in either orientation. Because flagellin phase variation is a relatively infrequent event in *Salmonella*, the expression level of Hin is likely to be kept relatively low. Recently, STM0347, a homolog of CsgD, has been shown to significantly reduce the probability of Hin-mediated DNA inversion by suppressing Hin expression to a relatively low level (227).

FLAGELLAR ASSEMBLY

Morphological assembly pathway. Flagellar assembly proceeds from more proximal to more distal structures (71, 72). The MS ring is the first structure in flagellar formation. FliF can self-assemble into the MS ring in the cytoplasmic membrane (18, 72), but FliG is required for efficient and robust MS-ring formation (228). The assembly of the transmembrane export gate complex begins with the formation of the FliP₅-FliR₁ complex with the help of the FliO protein (229, 230). Four FliQ subunits assemble into the FliP₅-FliR complex to form the FliP₅-FliQ₄-FliR₁ complex with a helical subunit

array (159). Next, a single copy of FlhB surrounds the FliP₅-FliQ₄-FliR₁ complex (160), and finally, nine FlhA subunits assemble around the FlhB₁-FliP₅-FliQ₄-FliR₁ complex during MS-ring formation to form the export gate complex inside the MS ring (228). FliG self-assembles into the FliG ring on the cytoplasmic face of the MS ring, and the FliM₁-FliN₃ complex then binds to each FliG subunit in the FliG ring to form the C ring (31). Upon the completion of the C-ring structure, FliH, FliI, and FliJ assemble into the cytoplasmic ATPase ring complex at the base of the flagellum, and this ATPase ring complex is anchored to the C ring through interactions between FliH and FliN (141). Once the export gate complex is activated by ATP hydrolysis by the cytoplasmic ATPase ring complex, the activated export gate complex efficiently utilizes PMF to unfold and transport flagellar axial proteins. FliE is the first export substrate transported by the σ^{54} and self-assembles at the tip of the FliP₅-FliR₁ helical structure to form the FliE zone. The interactions of FliE subunits with FliP and FliR fully open the exit gate of the polypide channel, allowing other axial proteins to diffuse down the central channel of the growing axial structure. At the tip of the FliE zone, FlgB, FlgC, FlgF, and FlgG subunits assemble in this order to form the rod (22, 23). FlgJ serves as the rod cap at the rod tip not only to support rod assembly but also to locally digest the PG layer, allowing the rod to penetrate the PG layer (120, 128). Once the distal rod structure is complete, FlgI and FlgH assemble around the distal rod in the PG layer and the outer membrane, respectively, forming the LP-ring complex (65). Upon the completion of the LP ring, the rod cap dissociates from the rod tip (129), and FlgD self-assembles into the hook cap at the rod tip. Through the action of the hook cap, the newly transported FlgE monomer is efficiently folded and incorporated into the growing end of the hook structure (121, 127). When the hook reaches its mature length of about 55 nm in *Salmonella*, the hook cap is replaced by FlgK (121). FlgK self-assembles at the hook tip, and FlgL then self-assembles at the tip of the FlgK zone to form the hook-filament junction structure (111, 112). FliD self-assembles into the filament cap at the tip of the junction structure and promotes the assembly of flagellin molecules at the distal end of the growing filament structure, allowing the filament to grow to approximately 15 μ m in length (123).

The σ^{54} coordinates flagellar protein export and assembly. The *Salmonella* σ^{54} transports 14 different proteins from the cytoplasm while monitoring the

construction of the HBB structure. These 14 export substrates are classified into two export classes: one is the rod-type (FliE, FlgB, FlgC, FlgF, FlgG, and FlgJ) and hook-type (FlgD, FlgE, and FliK) class needed for the structure and assembly of the rod and hook, and the other is the filament-type class (FlgK, FlgL, FlgM, FliD, and FliC) responsible for filament formation at the hook tip (231, 232). During HBB assembly, the σ^{54} acts specifically on the rod-hook-type substrates. When the length of the hook reaches about 55 nm in *Salmonella*, the σ^{54} switches its substrate specificity from the rod-hook type to the filament type (233, 234). As a result, hook assembly terminates, and filament assembly initiates (Fig. 13). At that time, the σ^{54} secretes FlgM into the culture medium, allowing FliA to induce transcription from class 3 promoters (212, 213). Thus, by switching the substrate specificity of the σ^{54} , the expression hierarchy of flagellar genes can be precisely paralleled with the flagellar assembly process (Fig. 12).

Hook length control and substrate specificity switching. The length of the hook structure is controlled at about 55 nm (± 6 nm) in wild-type *Salmonella* cells (80). Short hooks are too stiff to function as universal joints, whereas long hooks somehow destabilize the flagellar bundle structure compared to wild-type hooks (235). This suggests that the control of the hook length is critical for the hook to function properly as a universal joint. Therefore, there must be something that measures the hook length and signals the σ^{54} to stop rod-hook-type protein export and initiate filament-type protein export. At least three flagellar proteins, FliK, FlhA, and FlhB, are directly involved in the substrate specificity switching of the σ^{54} (Fig. 13). When this switching event is inhibited by certain mutations in either *fliK*, *flhB*, or *flhA*, the σ^{54} continues to transport FlgE subunits to the distal end of the growing hook structure, forming an unusually elongated hook called a polyhook (8).

FliK is secreted during hook assembly and controls the length of the hook structure (236). FliK consists of an N-terminal domain (FliK_N) (residues 1 to 207), a C-terminal domain (FliK_C) (residues 268 to 405), and a flexible linker region (FliK_L) (residues 208 to 267) connecting these two domains (237). FliK_N has an unstable and flexible conformation (238) and functions as a molecular ruler that

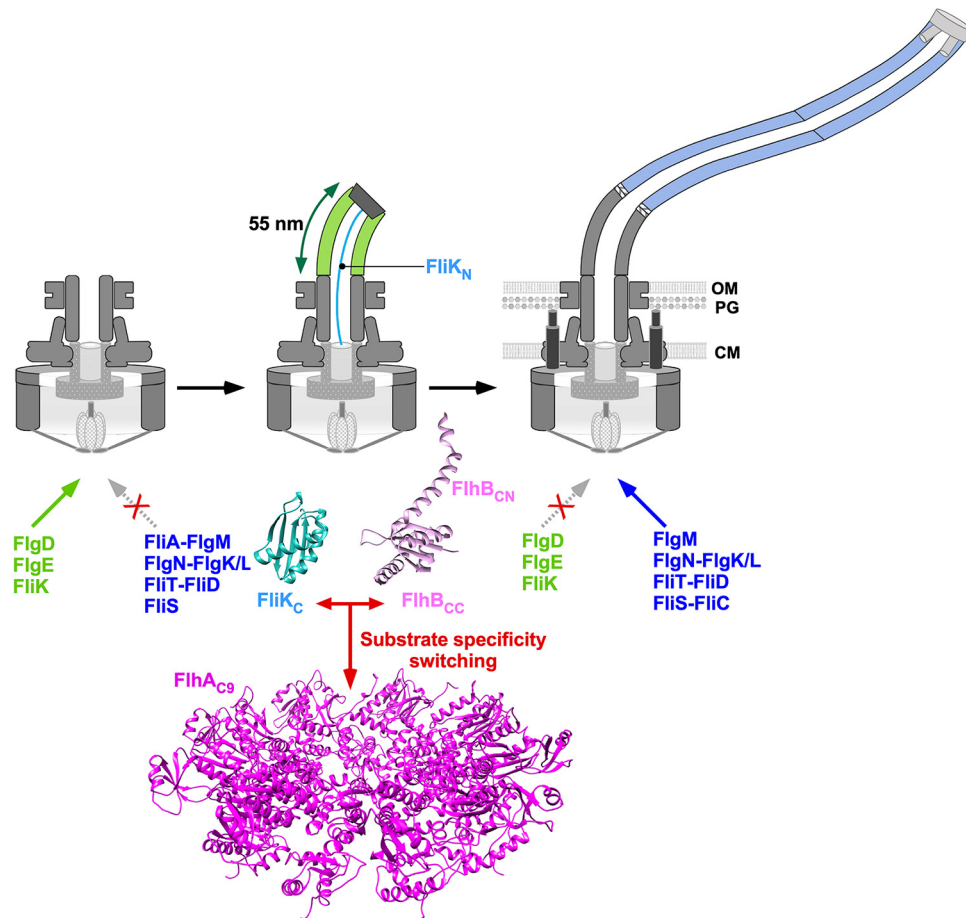


FIG 13 Model for the substrate specificity switching of the ft3SS. The ft3SS transports the hook-type export substrates FlgD, FlgE, and FliK during hook assembly but does not transport the filament-type substrates FlgK/L, FlgM, and FliD, which form a complex with FlgN, FliA, and FliT in the cytoplasm, respectively. At that point, no flagellin molecules (FliC and FljB) are expressed. When the hook length reaches about 55 nm, the C-terminal domain of FliK (FliK_C) binds to FlhB_{CC} to induce a conformational change of a cleaved form of FlhB_C. Next, the FliK_C-FlhB_C complex binds to FlhA_C to induce the remodeling of the FlhA_C ring structure, allowing the ft3SS to terminate the export of hook-type proteins and initiate the export of filament-type proteins.

measures the hook length through its interactions with the hook cap and the inner surface of the hook (239–241). FliK_C is divided into two structural parts: a compactly folded domain (residues 268 to 352) responsible for the interaction with FlhB_C and an intrinsically disordered C-terminal tail (FliK_{CT}) (residues 353 to 405) (242). The interaction between the core domain of FliK_C and FlhB_C is a critical step in the substrate specificity switching of the ft3SS, and FliK_{CT} regulates the FliK_C-FlhB_C interaction during hook assembly (243, 244). FliK_L is important not only for the proper control of the hook length but also for the switching of the substrate specificity of the ft3SS at an appropriate time for hook assembly (245).

FlhB_C serves as a switching device that changes the substrate specificity of the ft3SS from the rod-hook type to the filament type. FlhB_C undergoes autocatalytic cleavage between Asn269 and Pro270 in the highly conserved NPTH motif, producing two distinct FlhB_{CN} (residues 211 to 269) and FlhB_{CC} (residues 270 to 383) polypeptides (162, 246). The N-terminal region of FlhB_{CN} (residues 211 to 228) adopts a very flexible conformation and is likely to act as a linker connecting FlhB_{TM} and FlhB_C. Residues 229 to 269 form a single α -helix, and the C-terminal region of this helix is inserted deeply into the hydrophobic core of FlhB_{CC} (247). The *flhB(N269A)* and *flhB(P270A)* mutations not

only inhibit the autocleavage of FlhB_C but also prevent the fT3SS from switching its substrate specificity, thereby producing polyhooks with or without filament attachment (248). Photo-cross-linking experiments have shown that these two mutations do not affect the binding of FliK_C to FlhB_C (249). A conserved hydrophobic patch formed by the Ala286, Pro287, Ala341, and Leu344 residues in FlhB_{CC} is involved in the interaction of FlhB_C with the N-terminal segment of the hook-type protein that contains an export signal recognized by the fT3SS (163). Because polyhooks produced by the *flhB(N269A)* and *flhB(P270A)* mutants are significantly shorter than the average length of polyhooks produced by the *fliK*-null mutant (249), the interaction between FliK_C and FlhB_C with either the N269A or P270A substitution seems to induce a structural rearrangement of this conserved hydrophobic patch, thereby reducing the hook polymerization rate considerably. The *flhA(A489E)* suppressor mutation in FlhA_C allows the *flhB(P270A)* mutant to initiate filament assembly more efficiently. However, this *flhA* mutation does not significantly shorten the polyhook length (249). Therefore, these observations suggest that the autocleavage of FlhB_C is required not only for an FliK-dependent conformational change of FlhB_C that is responsible for the efficient termination of hook assembly but also for a conformational change of FlhA_C that is responsible for the initiation of filament assembly.

As mentioned above, the FlhA_{C9} ring provides docking sites for the FlgN-FlgK/L, FliS-FliC, and FliT-FliD chaperone-substrate complexes, thereby facilitating the export of filament-type proteins by the fT3SS (170). FlhA_C consists of four domains, D1, D2, D3, and D4 (182). The chaperone-binding site is located at the interface between domains D1 and D2 of FlhA_C, and the well-conserved residues Asp456, Phe459, and Thr490 in the chaperone-binding site are directly involved in the interaction of FlhA_C with the flagellar chaperones (169, 179). Because the *flhA(A489E)* suppressor mutation is located in the chaperone-binding site of FlhA_C, this mutation seems to induce a conformational change of this chaperone-binding site (249), thereby allowing the filament-type export substrates to be more efficiently transported by the fT3SS with the *flhB(P270A)* mutation.

High-speed atomic force microscopy has revealed that the Glu351, Trp354, and Asp356 residues in the C-terminal region of FlhA_L bind to the D1 and D3 domains of the adjacent FlhA_C subunit in the FlhA_{C9} ring, thereby stabilizing

the ring structure considerably (250). This has been confirmed by a recent high-resolution cryoEM image analysis of *Vibrio* FlhA (251). FlhA_C with either the W354A, E351A/D356A, or E351A/W354A/D356A substitution not only inhibits FlhA_{C9} ring formation but also reduces the binding affinity of FlhA_C for the FlgN-FlgK chaperone-substrate complex. These *flhA* mutants produce no filaments at the hook tip. Therefore, these observations suggest that interactions of the C-terminal portion of FlhA_L, including Glu351, Trp354, and Asp356, with its neighboring FlhA_C subunit in the FlhA_{C9} ring are required for the initiation of filament-type protein export upon the completion of hook assembly (250). The crystal structure of FlhA_C with the E351A/D356A double mutation has shown that the C-terminal region of FlhA_L with this double mutation binds to the chaperone-binding site in FlhA_C. Since the removal of the entire FlhA_L sequence increases the binding affinity of FlhA_C for the FlgN chaperone compared with FlhA_C with either the E351A/D356A or E351A/W354A/D356A substitution, the binding of the C-terminal portion of FlhA_L to the chaperone-binding site in FlhA_C seems to suppress the premature docking of the chaperone-substrate complex to each FlhA_C subunit in the ring during hook assembly (171). Thus, the FliK_C-FlhB_C interaction is postulated to cause a remodeling of the FlhA_{C9} ring structure, with the C-terminal region of each FlhA_L subunit dissociating from the chaperone-binding site of FlhA_C and binding to the D1 and D3 domains of its neighboring FlhA_C subunit in the ring. As a result, the chaperone-substrate complexes can bind to each FlhA_C subunit in the ring, allowing filament formation at the hook tip (Fig. 13).

CONCLUSIONS AND PERSPECTIVES

Most of the proteins that make up the flagellum have been revealed at an atomic resolution by X-ray crystallography. In addition, recent high-resolution cryoEM image analyses have provided deep insights into the assembly and function of the MS ring, the rod, the LP ring, the hook, the filament, the filament cap, and the force generator. Thus, flagellar assembly and operation mechanisms can now be discussed at the level of atomic structures. Since high-resolution structures of the CCW and CW states of the C ring have not yet been obtained, it is unclear how the chemotaxis signal received by the FliM subunits in the C ring is transmitted to the FliG subunits in the upper part of the C ring and induces the highly cooperative remodeling of the C ring that is responsible for the directional switching of the flagellar motor. A more precise understanding of the

mechanism of flagellar motor rotation will require biophysical and molecular genetic approaches based on the atomic model of the flagellar motor complex.

The transmembrane export gate complex has a dual-fuel protein export engine, a membrane voltage sensor, a polypeptide channel, and a substrate-docking platform. Because there is no structural information on FlhA_{TM} acting as a dual-ion channel, it remains unknown how FlhA_{TM} associates with the FliP₅-FliQ₄-FliR₁-FlhB₁ complex inside the MS ring, how FlhA_{TM} can conduct H⁺ and Na⁺ of different ionic radii, what the membrane voltage sensor is, and how the export gate complex acts as a cation/protein antiporter that couples inward-directed cation flow with outward-directed protein translocation. In order to elucidate the energy-coupling mechanism of the fT3SS, the overall structure of the fT3SS in different states of flagellar protein export must be revealed by high-resolution cryoEM image analysis.

ACKNOWLEDGMENTS

We acknowledge Keiichi Namba for continuous support and encouragement.

This work was supported in part by JSPS KAKENHI grants JP19H03182, JP22H02573, and JP22K19274 (to T.M.) and JP20K15749 and JP22K06162 (to M.K.) and MEXT KAKENHI grants JP20H0553 and JP22H04844 (to T.M.).

REFERENCES

1. Minamino T, Imada K. 2015. The bacterial flagellar motor and its structural diversity. *Trends Microbiol* 23:267–274. <https://doi.org/10.1016/j.tim.2014.12.011>.
2. Terashima H, Kawamoto A, Morimoto YV, Imada K, Minamino T. 2017. Structural differences in the bacterial flagellar motor among bacterial species. *Biophys Physicobiol* 14:191–198. https://doi.org/10.2142/biophysico.14.0_191.
3. Macnab RM. 1996. Flagella and motility, p 123–145. In Neidhardt FC, Curtiss R, III, Ingraham JL, Lin ECC, Low KB, Magasanik B, Reznikoff WS, Riley M, Schaechter M, Umberger HE (ed), *Escherichia coli and Salmonella typhimurium: cellular and molecular biology*, 2nd ed. ASM Press, Washington, DC.
4. Macnab RM. 2003. How bacteria assemble flagella. *Annu Rev Microbiol* 57:77–100. <https://doi.org/10.1146/annurev.micro.57.030502.090832>.
5. Minamino T, Namba K. 2004. Self-assembly and type III protein export of the bacterial flagellum. *J Mol Microbiol Biotechnol* 7:5–17. <https://doi.org/10.1159/000077865>.
6. Berg HC. 2003. The rotary motor of bacterial flagella. *Annu Rev Biochem* 72:19–54. <https://doi.org/10.1146/annurev.biochem.72.121801.161737>.
7. Chevance FFV, Hughes KT. 2008. Coordinating assembly of a bacterial macromolecular machine. *Nat Rev Microbiol* 6:455–465. <https://doi.org/10.1038/nrmicro1887>.
8. Minamino T. 2018. Hierarchical protein export mechanism of the bacterial flagellar type III protein export apparatus. *FEMS Microbiol Lett* 365:fny117. <https://doi.org/10.1093/femsle/fny117>.
9. Homma M, Kojima S. 2022. The periplasmic domain of the ion-conducting stator of bacterial flagella regulates force generation. *Front Microbiol* 13:869187. <https://doi.org/10.3389/fmicb.2022.869187>.
10. Hu H, Santiveri M, Wadhwa N, Berg HC, Erhardt M, Taylor NMI. 2022. Structural basis of torque generation in the bi-directional bacterial flagellar motor. *Trends Biochem Sci* 47:160–172. <https://doi.org/10.1016/j.tibs.2021.06.005>.
11. Manson MD. 2022. Rotary nanomotors in the rear view mirror. *Front Microbiol* 13:873573. <https://doi.org/10.3389/fmicb.2022.873573>.
12. Minamino T, Kinoshita M, Namba K. 2022. Insight into distinct functional roles of the flagellar ATPase complex for flagellar assembly in *Salmonella*. *Front Microbiol* 13:864178. <https://doi.org/10.3389/fmicb.2022.864178>.
13. Minamino T, Kinoshita M, Morimoto YV, Namba K. 2022. Activation mechanism of the bacterial flagellar dual-fuel protein export engine. *Biophys Physicobiol* 19:e190046. <https://doi.org/10.2142/biophysico.bppb-v19.0046>.
14. Mondino S, San Martin F, Buschiazzo A. 2022. 3D cryo-EM imaging of bacterial flagella: novel structural and mechanistic insights into cell motility. *J Biol Chem* 298:102105. <https://doi.org/10.1016/j.jbc.2022.102105>.
15. Rieu M, Krutyholowa R, Taylor NMI, Berry RM. 2022. A new class of biological ion-driven rotary molecular motors with 5:2 symmetry. *Front Microbiol* 13:948383. <https://doi.org/10.3389/fmicb.2022.948383>.
16. Morimoto YV, Minamino T. 2014. Structure and function of the bi-directional bacterial flagellar motor. *Biomolecules* 4:217–234. <https://doi.org/10.3390/biom4010217>.
17. Nakamura S, Minamino T. 2019. Flagella-driven motility of bacteria. *Biomolecules* 9:279. <https://doi.org/10.3390/biom9070279>.
18. Ueno T, Oosawa K, Aizawa S-I. 1992. M ring, S ring and proximal rod of the flagellar basal body of *Salmonella typhimurium* are composed of subunits of a single protein, FliF. *J Mol Biol* 227:672–677. [https://doi.org/10.1016/0022-2836\(92\)90216-7](https://doi.org/10.1016/0022-2836(92)90216-7).
19. Ueno T, Oosawa K, Aizawa S-I. 1994. Domain structures of the MS ring component protein (FliF) of the flagellar basal body of *Salmonella typhimurium*. *J Mol Biol* 236:546–555. <https://doi.org/10.1006/jmbi.1994.1164>.
20. Minamino T, Imada K, Namba K. 2008. Molecular motors of the bacterial flagella. *Curr Opin Struct Biol* 18:693–701. <https://doi.org/10.1016/j.sbi.2008.09.006>.
21. Suzuki H, Yonekura K, Namba K. 2004. Structure of the rotor of the bacterial flagellar motor revealed by electron cryomicroscopy and single-particle image analysis. *J Mol Biol* 337:105–113. <https://doi.org/10.1016/j.jmb.2004.01.034>.
22. Johnson S, Furlong EJ, Deme JC, Nord AL, Caesar JJE, Chevance FFV, Berry RM, Hughes KT, Lea SM. 2021. Molecular structure of the intact bacterial flagellar basal body. *Nat Microbiol* 6:712–721. <https://doi.org/10.1038/s41564-021-00895-y>.
23. Tan J, Zhang X, Wang X, Xu C, Chang S, Wu H, Wang T, Liang H, Gao H, Zhou Y, Zhu Y. 2021. Structural basis of assembly and torque transmission of the bacterial flagellar motor. *Cell* 184:2665–2679.e19. <https://doi.org/10.1016/j.cell.2021.03.057>.
24. Kawamoto A, Miyata T, Makino F, Kinoshita M, Minamino T, Imada K, Kato T, Namba K. 2021. Native flagellar MS ring is formed by 34 subunits with 23-fold and 11-fold subsymmetries. *Nat Commun* 12:4223. <https://doi.org/10.1038/s41467-021-24507-9>.
25. Johnson S, Fong YH, Deme JC, Furlong EJ, Kuhlen L, Lea SM. 2020. Symmetry mismatch in the MS-ring of the bacterial flagellar rotor explains the structural coordination of secretion and rotation. *Nat Microbiol* 5:966–975. <https://doi.org/10.1038/s41564-020-0703-3>.

26. Takekawa N, Kawamoto A, Sakuma M, Kato T, Kojima S, Kinoshita M, Minamino T, Namba K, Homma M, Imada K. 2021. Two distinct conformations in 34 FliF subunits generate three different symmetries within the flagellar MS-ring. *mBio* 12:e03199-20. <https://doi.org/10.1128/mBio.03199-20>.
27. Yamaguchi S, Aizawa S, Kihara M, Isomura M, Jones CJ, Macnab RM. 1986. Genetic evidence for a switching and energy-transducing complex in the flagellar motor of *Salmonella typhimurium*. *J Bacteriol* 168:1172–1179. <https://doi.org/10.1128/jb.168.3.1172-1179.1986>.
28. Sockett H, Yamaguchi S, Kihara M, Irikura VM, Macnab RM. 1992. Molecular analysis of the flagellar switch protein FliM of *Salmonella typhimurium*. *J Bacteriol* 174:793–806. <https://doi.org/10.1128/jb.174.3.793-806.1992>.
29. Irikura VM, Kihara M, Yamaguchi S, Sockett H, Macnab RM. 1993. *Salmonella typhimurium* fliG and fliN mutations causing defects in assembly, rotation, and switching of the flagellar motor. *J Bacteriol* 175:802–810. <https://doi.org/10.1128/jb.175.3.802-810.1993>.
30. Khan S, Khan IH, Reese TS. 1991. New structural features of the flagellar base in *Salmonella typhimurium* revealed by rapid-freeze electron microscopy. *J Bacteriol* 173:2888–2896. <https://doi.org/10.1128/jb.173.9.2888-2896.1991>.
31. Francis NR, Sosinsky GE, Thomas D, DeRosier DJ. 1994. Isolation, characterization, and structure of bacterial flagellar motors containing the switch complex. *J Mol Biol* 235:1261–1270. <https://doi.org/10.1006/jmbi.1994.1079>.
32. Thomas DR, Morgan DG, DeRosier DJ. 1999. Rotational symmetry of the C ring and a mechanism for the flagellar rotary motor. *Proc Natl Acad Sci U S A* 96:10134–10139. <https://doi.org/10.1073/pnas.96.18.10134>.
33. Thomas DR, Francis NR, Xu C, DeRosier DJ. 2006. The three-dimensional structure of the flagellar rotor from a clockwise-locked mutant of *Salmonella enterica* serovar Typhimurium. *J Bacteriol* 188:7039–7048. <https://doi.org/10.1128/JB.00552-06>.
34. Sakai T, Miyata T, Terahara N, Mori K, Inoue Y, Morimoto YV, Kato T, Namba K, Minamino T. 2019. Novel insights into conformational rearrangements of the bacterial flagellar switch complex. *mBio* 10:e00079-19. <https://doi.org/10.1128/mBio.00079-19>.
35. Lee LK, Ginsburg MA, Crovace C, Donohoe M, Stock D. 2010. Structure of the torque ring of the flagellar motor and the molecular basis for rotational switching. *Nature* 466:996–1000. <https://doi.org/10.1038/nature09300>.
36. Francis NR, Irikura VM, Yamaguchi S, DeRosier DJ, Macnab RM. 1992. Localization of the *Salmonella typhimurium* flagellar switch protein FliG to the cytoplasmic M-ring face of the basal body. *Proc Natl Acad Sci U S A* 89:6304–6308. <https://doi.org/10.1073/pnas.89.14.6304>.
37. Kihara M, Miller GU, Macnab RM. 2000. Deletion analysis of the flagellar switch protein FliG of *Salmonella*. *J Bacteriol* 182:3022–3028. <https://doi.org/10.1128/JB.182.11.3022-3028.2000>.
38. Lynch MJ, Levenson R, Kim EA, Sircar R, Blair DF, Dahlquist FW, Crane BR. 2017. Co-folding of a FliF-FliG split domain forms the basis of the MS:C ring interface within the bacterial flagellar motor. *Structure* 25:317–328. <https://doi.org/10.1016/j.str.2016.12.006>.
39. Baker MAB, Hynson RMG, Ganuelas LA, Mohammadi NS, Liew CW, Rey AA, Duff AP, Whitten AE, Jeffries CM, Delalez NJ, Morimoto YV, Stock D, Armitage JP, Turberfield AJ, Namba K, Berry RM, Lee LK. 2016. Domain-swap polymerization drives the self-assembly of the bacterial flagellar motor. *Nat Struct Mol Biol* 23:197–203. <https://doi.org/10.1038/nsmb.3172>.
40. Kim EA, Panushka J, Meyer T, Carlisle R, Baker S, Ide N, Lynch M, Crane BR, Blair DF. 2017. Architecture of the flagellar switch complex of *Escherichia coli*: conformational plasticity of FliG and implications for adaptive remodelling. *J Mol Biol* 429:1305–1320. <https://doi.org/10.1016/j.jmb.2017.02.014>.
41. Kinoshita M, Namba K, Minamino T. 2018. Effect of a clockwise-locked deletion in FliG on the FliG ring structure of the bacterial flagellar motor. *Genes Cells* 23:241–247. <https://doi.org/10.1111/gtc.12565>.
42. Zhou J, Lloyd SA, Blair DF. 1998. Electrostatic interactions between rotor and stator in the bacterial flagellar motor. *Proc Natl Acad Sci U S A* 95:6436–6441. <https://doi.org/10.1073/pnas.95.11.6436>.
43. Morimoto YV, Nakamura S, Kami-ike N, Namba K, Minamino T. 2010. Charged residues in the cytoplasmic loop of MotA are required for stator assembly into the bacterial flagellar motor. *Mol Microbiol* 78:1117–1129. <https://doi.org/10.1111/j.1365-2958.2010.07391.x>.
44. Mathews MA, Tang HL, Blair DF. 1998. Domain analysis of the FliM protein of *Escherichia coli*. *J Bacteriol* 180:5580–5590. <https://doi.org/10.1128/JB.180.21.5580-5590.1998>.
45. Park S-Y, Lowder B, Bilwes AM, Blair DF, Crane BR. 2006. Structure of FliM provides insight into assembly of the switch complex in the bacterial flagella motor. *Proc Natl Acad Sci U S A* 103:11886–11891. <https://doi.org/10.1073/pnas.0602811103>.
46. Paul K, Gonzalez-Bonet G, Bilwes AM, Crane BR, Blair D. 2011. Architecture of the flagellar rotor. *EMBO J* 30:2962–2971. <https://doi.org/10.1038/emboj.2011.188>.
47. McDowell MA, Marcoux J, McVicker G, Johnson S, Fong YH, Stevens R, Bowman LAH, Degiacomi MT, Yan J, Wise A, Friede ME, Benesch JLP, Deane JE, Tang CM, Robinson CV, Lea SM. 2016. Characterisation of *Shigella* Spa33 and *Thermotoga* FliM/N reveals a new model for C-ring assembly in T3SS. *Mol Microbiol* 99:749–766. <https://doi.org/10.1111/mmi.13267>.
48. Delalez NJ, Wadhams GH, Rosser G, Xue Q, Brown MT, Dobbie IM, Berry RM, Leake MC, Armitage JP. 2010. Signal-dependent turnover of the bacterial flagellar switch protein FliM. *Proc Natl Acad Sci U S A* 107:11347–11351. <https://doi.org/10.1073/pnas.1000284107>.
49. Lele PP, Branch RW, Nathan VS, Berg HC. 2012. Mechanism for adaptive remodeling of the bacterial flagellar switch. *Proc Natl Acad Sci U S A* 109:20018–20022. <https://doi.org/10.1073/pnas.1212327109>.
50. Delalez NJ, Berry RM, Armitage JP. 2014. Stoichiometry and turnover of the bacterial flagellar switch protein FliN. *mBio* 5:e01216-14. <https://doi.org/10.1128/mBio.01216-14>.
51. Lele PP, Shrivastava A, Roland T, Berg HC. 2015. Response thresholds in bacterial chemotaxis. *Sci Adv* 1:e1500299. <https://doi.org/10.1126/sciadv.1500299>.
52. Lee S-Y, Cho HS, Pelton JG, Yan D, Henderson RK, King DS, Huang L, Kustu S, Berry EA, Wemmer DE. 2001. Crystal structure of an activated response regulator bound to its target. *Nat Struct Biol* 8:52–56. <https://doi.org/10.1038/83053>.
53. Sarkar MK, Paul K, Blair D. 2010. Chemotaxis signaling protein CheY binds to the rotor protein FliN to control the direction of flagellar rotation in *Escherichia coli*. *Proc Natl Acad Sci U S A* 107:9370–9375. <https://doi.org/10.1073/pnas.1000935107>.
54. Afanar O, Di Paolo D, Eisenstein M, Levi K, Plochowitz A, Kapanidis AN, Berry RM, Eisenbach M. 2021. The switching mechanism of the bacterial rotary motor combines tight regulation with inherent flexibility. *EMBO J* 40:e104683. <https://doi.org/10.15252/embj.2020104683>.
55. Lloyd SA, Whitby FG, Blair DF, Hill CP. 1999. Structure of the C-terminal domain of FliG, a component of the rotor in the bacterial flagellar motor. *Nature* 400:472–475. <https://doi.org/10.1038/22794>.
56. Morimoto YV, Nakamura S, Hiraoka KD, Namba K, Minamino T. 2013. Distinct roles of highly conserved charged residues at the MotA-FliG interface in bacterial flagellar motor rotation. *J Bacteriol* 195:474–481. <https://doi.org/10.1128/JB.01971-12>.

57. Lam K-H, Ip W-S, Lam Y-W, Chan S-O, Ling TK-W, Au SW-N. 2012. Multiple conformations of the FlgG C-terminal domain provide insight into flagellar motor switching. *Structure* 20:315–325. <https://doi.org/10.1016/j.str.2011.11.020>.
58. Paul K, Brunstetter D, Titen S, Blair DF. 2011. A molecular mechanism of direction switching in the flagellar rotation of *Escherichia coli*. *Proc Natl Acad Sci U S A* 108:17171–17176. <https://doi.org/10.1073/pnas.1110111108>.
59. Vartanian AS, Paz A, Fortgang EA, Abramson J, Dahlquist FW. 2012. Structure of flagellar motor proteins in complex allows for insights into motor structure and switching. *J Biol Chem* 287:35779–35783. <https://doi.org/10.1074/jbc.C112.378380>.
60. Van Way SM, Millas SG, Lee AH, Manson MD. 2004. Rusty, jammed, and well-oiled hinges: mutations affecting the interdomain region of FlgG, a rotor element of the *Escherichia coli* flagellar motor. *J Bacteriol* 186:3173–3181. <https://doi.org/10.1128/JB.186.10.3173-3181.2004>.
61. Togashi F, Yamaguchi S, Kihara M, Aizawa S-I, Macnab RM. 1997. An extreme clockwise switch bias mutation in *fliG* of *Salmonella typhimurium* and its suppression by slow-motile mutations in *motA* and *motB*. *J Bacteriol* 179:2994–3003. <https://doi.org/10.1128/jb.179.9.2994-3003.1997>.
62. Minamino T, Imada K, Kinoshita M, Nakamura S, Morimoto YV, Namba K. 2011. Structural insight into the rotational switching mechanism of the bacterial flagellar motor. *PLoS Biol* 9:e1000616. <https://doi.org/10.1371/journal.pbio.1000616>.
63. Minamino T, Kinoshita M, Namba K. 2019. Directional switching mechanism of the bacterial flagellar motor. *Comput Struct Biotechnol J* 17:1075–1081. <https://doi.org/10.1016/j.csbj.2019.07.020>.
64. Kinoshita M, Furukawa Y, Uchiyama S, Imada K, Namba K, Minamino T. 2018. Insight into adaptive remodeling of the rotor ring complex of the bacterial flagellar motor. *Biochem Biophys Res Commun* 496:12–17. <https://doi.org/10.1016/j.bbrc.2017.12.118>.
65. Yamaguchi T, Makino F, Miyata T, Minamino T, Kato T, Namba K. 2021. Structure of the molecular bushing of the bacterial flagellar motor. *Nat Commun* 12:4469. <https://doi.org/10.1038/s41467-021-24715-3>.
66. Jones CJ, Homma M, Macnab RM. 1989. L-, P-, and M-ring proteins of the flagellar basal body of *Salmonella typhimurium*: gene sequences and deduced protein sequences. *J Bacteriol* 171:3890–3900. <https://doi.org/10.1128/jb.171.7.3890-3900.1989>.
67. Hizukuri Y, Yakushi T, Kawagishi I, Homma M. 2006. Role of the intramolecular disulfide bond in FlgI, the flagellar P-ring component of *Escherichia coli*. *J Bacteriol* 188:4190–4197. <https://doi.org/10.1128/JB.01896-05>.
68. Nambu T, Kutsukake K. 2000. The *Salmonella* FlgA protein, a putative periplasmic chaperone essential for flagellar P ring formation. *Microbiology (Reading)* 146:1171–1178. <https://doi.org/10.1099/00221287-146-5-1171>.
69. Matsunami H, Yoon Y-H, Meshcheryakov VA, Namba K, Samatey FA. 2016. Structural flexibility of the periplasmic protein, FlgA, regulate flagellar P-ring assembly in *Salmonella enterica*. *Sci Rep* 6:27399. <https://doi.org/10.1038/srep27399>.
70. Chevance FFV, Takahashi N, Karlinsey JE, Gnerer J, Hirano T, Samudrala R, Aizawa S-I, Hughes KT. 2007. The mechanism of outer membrane penetration by the eubacterial flagellum and implications for spirochete evolution. *Genes Dev* 21:2326–2335. <https://doi.org/10.1101/gad.1571607>.
71. Suzuki T, Iino T, Horiguchi T, Yamaguchi S. 1978. Incomplete flagellar structures in nonflagellate mutants of *Salmonella typhimurium*. *J Bacteriol* 133:904–915. <https://doi.org/10.1128/jb.133.2.904-915.1978>.
72. Kubori T, Shimamoto N, Yamaguchi S, Namba K, Aizawa S-I. 1992. Morphological pathway of flagellar assembly in *Salmonella typhimurium*. *J Mol Biol* 226:433–446. [https://doi.org/10.1016/0022-2836\(92\)90958-m](https://doi.org/10.1016/0022-2836(92)90958-m).
73. Imada K. 2018. Bacterial flagellar axial structure and its construction. *Biophys Rev* 10:559–570. <https://doi.org/10.1007/s12551-017-0378-z>.
74. Okino H, Isomura M, Yamaguchi S, Magariyama Y, Kudo S, Aizawa S-I. 1989. Release of flagellar filament-hook-rod complex by a *Salmonella typhimurium* mutant defective in the M ring of the basal body. *J Bacteriol* 171:2075–2082. <https://doi.org/10.1128/jb.171.4.2075-2082.1989>.
75. Minamino T, Yamaguchi S, Macnab RM. 2000. Interaction between FlIE and FlgB, a proximal rod component of the flagellar basal body of *Salmonella*. *J Bacteriol* 182:3029–3036. <https://doi.org/10.1128/JB.182.11.3029-3036.2000>.
76. Hendriksen JJ, Lee HJ, Bradshaw AJ, Namba K, Chevance FFV, Minamino T, Hughes KT. 2021. Genetic analysis of the *Salmonella* FlIE protein that forms the base of the flagellar axial structure. *mBio* 12:e02392-21. <https://doi.org/10.1128/mBio.02392-21>.
77. Fujii T, Kato T, Hiraoka KD, Miyata T, Minamino T, Chevance FFV, Hughes KT, Namba K. 2017. Identical folds used for distinct mechanical functions of the bacterial flagellar rod and hook. *Nat Commun* 8:14276. <https://doi.org/10.1038/ncomms14276>.
78. Saijo-Hamano Y, Matsunami H, Namba K, Imada K. 2019. Architecture of the bacterial flagellar distal rod and hook of *Salmonella*. *Biomolecules* 9:260. <https://doi.org/10.3390/biom9070260>.
79. Brown MT, Steel BC, Silvestrin C, Wilkinson DA, Delalez NJ, Lumb CN, Obara B, Armitage JP, Berry RM. 2012. Flagellar hook flexibility is essential for bundle formation in swimming *Escherichia coli* cells. *J Bacteriol* 194:3495–3501. <https://doi.org/10.1128/JB.00209-12>.
80. Hirano T, Yamaguchi S, Oosawa K, Aizawa S-I. 1994. Roles of FlkK and FlhB in determination of flagellar hook length in *Salmonella typhimurium*. *J Bacteriol* 176:5439–5449. <https://doi.org/10.1128/jb.176.17.5439-5449.1994>.
81. Samatey FA, Matsunami H, Imada K, Nagashima S, Shaikh TR, Thomas DR, Chen JZ, DeRosier DJ, Kitao A, Namba K. 2004. Structure of the bacterial flagellar hook and implication for the molecular universal joint mechanism. *Nature* 431:1062–1068. <https://doi.org/10.1038/nature02997>.
82. Fujii T, Kato T, Namba K. 2009. Specific arrangement of α -helical coiled coils in the core domain of the bacterial flagellar hook for the universal joint function. *Structure* 17:1485–1493. <https://doi.org/10.1016/j.str.2009.08.017>.
83. Moriya N, Minamino T, Imada K, Namba K. 2011. Genetic analysis of the bacterial hook-capping protein FlgD responsible for hook assembly. *Microbiology (Reading)* 157:1354–1362. <https://doi.org/10.1099/mic.0.047100-0>.
84. Moriya N, Minamino T, Ferris HU, Morimoto YV, Ashihara M, Kato T, Namba N. 2013. Role of the Dc domain of the bacterial hook protein FlgE in hook assembly and function. *Biophysic (Nagoya-shi)* 9:63–72. <https://doi.org/10.2142/biophysics.9.63>.
85. Sakai T, Inoue Y, Terahara N, Namba K, Minamino T. 2018. A triangular loop of domain D1 of FlgE is essential for hook assembly but not for the mechanical function. *Biochem Biophys Res Commun* 495:1789–1794. <https://doi.org/10.1016/j.bbrc.2017.12.037>.
86. Hiraoka KD, Morimoto YV, Inoue Y, Fujii T, Miyata T, Makino F, Minamino T, Namba K. 2017. Straight and rigid flagellar hook made by insertion of the FlgG specific sequence into FlgE. *Sci Rep* 7:46723. <https://doi.org/10.1038/srep46723>.
87. Horvath P, Kato T, Miyata T, Namba K. 2019. Structure of *Salmonella* flagellar hook reveals intermolecular domain interactions for the universal joint function. *Biomolecules* 9:462. <https://doi.org/10.3390/biom9090462>.
88. Kato S, Okamoto M, Asakura S. 1984. Polymorphic transformation of the flagellar polyhook from *Escherichia coli* and *Salmonella typhimurium*. *J Mol Biol* 173:463–476. [https://doi.org/10.1016/0022-2836\(84\)90391-7](https://doi.org/10.1016/0022-2836(84)90391-7).

89. Kato T, Makino F, Miyata T, Horvath P, Namba K. 2019. Structure of the native supercoiled flagellar hook as a universal joint. *Nat Commun* 10:5295. <https://doi.org/10.1038/s41467-019-13252-9>.
90. Shibata S, Matsunami H, Aizawa S-I, Wolf M. 2019. Torque transmission mechanism of the curved bacterial flagellar hook revealed by cryo-EM. *Nat Struct Mol Biol* 26:941–945. <https://doi.org/10.1038/s41594-019-0301-3>.
91. Yonekura K, Maki-Yonekura S, Namba K. 2003. Complete atomic model of the bacterial flagellar filament by electron cryomicroscopy. *Nature* 424:643–650. <https://doi.org/10.1038/nature01830>.
92. Beatson SA, Minamino T, Pallen MJ. 2006. Variation in bacterial flagellins: from sequence to structure. *Trends Microbiol* 14:151–155. <https://doi.org/10.1016/j.tim.2006.02.008>.
93. Macnab RM, Ornston MK. 1977. Normal-to-curly flagellar transitions and their role in bacterial tumbling. Stabilization of an alternative quaternary structure by mechanical force. *J Mol Biol* 112:1–30. [https://doi.org/10.1016/s0022-2836\(77\)80153-8](https://doi.org/10.1016/s0022-2836(77)80153-8).
94. Samatey FA, Imada K, Nagashima S, Vonderviszt F, Kumasaka T, Yamamoto M, Namba K. 2001. Structure of the bacterial flagellar protofilament and implications for a switch for supercoiling. *Nature* 410:331–337. <https://doi.org/10.1038/35066504>.
95. Kanto S, Okino H, Aizawa S-I, Yamaguchi S. 1991. Amino acids responsible for flagellar shape are distributed in terminal regions of flagellin. *J Mol Biol* 219:471–480. [https://doi.org/10.1016/0022-2836\(91\)90187-b](https://doi.org/10.1016/0022-2836(91)90187-b).
96. Kamiya R, Asakura S, Yamaguchi S. 1980. Formation of helical filaments by copolymerization of 2 types of straight flagellins. *Nature* 286:628–630. <https://doi.org/10.1038/286628a0>.
97. Hayashi F, Tomaru H, Furukawa E, Ikeda K, Fukano H, Oosawa K. 2013. Key amino acid residues involved in the transitions of L- to R-type protofilaments of the *Salmonella* flagellar filament. *J Bacteriol* 195:3503–3513. <https://doi.org/10.1128/JB.02091-12>.
98. Asakura S. 1970. Polymerization of flagellin and polymorphism of flagella. *Adv Biophys* 1:99–155.
99. Calladine CR. 1975. Construction of bacterial flagella. *Nature* 255:121–124. <https://doi.org/10.1038/255121a0>.
100. Calladine CR. 1976. Design requirements for the construction of bacterial flagella. *J Theor Biol* 57:469–489. [https://doi.org/10.1016/0022-5193\(76\)90016-3](https://doi.org/10.1016/0022-5193(76)90016-3).
101. Calladine CR. 1978. Change of waveform in bacterial flagella: the role of mechanics at the molecular level. *J Mol Biol* 118:457–479. [https://doi.org/10.1016/0022-2836\(78\)90285-1](https://doi.org/10.1016/0022-2836(78)90285-1).
102. Maki-Yonekura S, Yonekura K, Namba K. 2010. Conformational change of flagellin for polymorphic supercoiling of the flagellar filament. *Nat Struct Mol Biol* 17:417–422. <https://doi.org/10.1038/nsmb.1774>.
103. Kreutzberger MAB, Sonani RR, Liu J, Chatterjee S, Wang F, Sebastian AL, Biswas P, Ewing C, Zheng W, Poly F, Frankel G, Luisi BF, Calladine CR, Krupovic M, Scharf BE, Egelman EH. 2022. Convergent evolution in the supercoiling of prokaryotic flagellar filaments. *Cell* 185:3487–3500.e14. <https://doi.org/10.1016/j.cell.2022.08.009>.
104. Silverman M, Simon M. 1980. Phase variation: genetic analysis of switching mutants. *Cell* 19:845–854. [https://doi.org/10.1016/0092-8674\(80\)90075-6](https://doi.org/10.1016/0092-8674(80)90075-6).
105. Yamaguchi T, Toma S, Terahara N, Miyata T, Ashihara M, Minamino T, Namba K, Kato T. 2020. Structural and functional comparison of *Salmonella* flagellar filaments composed of FljB and FljC. *Biomolecules* 10:246. <https://doi.org/10.3390/biom10020246>.
106. Horstmann JA, Zschieschang E, Truschel T, de Diego J, Lunelli M, Rohde M, May T, Strowig T, Stradal T, Kolbe M, Erhardt M. 2017. Flagellin phase-dependent swimming on epithelial cell surfaces contributes to productive *Salmonella* gut colonisation. *Cell Microbiol* 19:e12739. <https://doi.org/10.1111/cmi.12739>.
107. Ambler RP, Rees MW. 1959. Epsilon-N-methyl-lysine in bacterial flagellar protein. *Nature* 184:56–57. <https://doi.org/10.1038/184056b0>.
108. Stocker BAD, McDonough MW, Ambler RP. 1961. A gene determining presence or absence of ϵ -N-methyl-lysine in *Salmonella* flagellar protein. *Nature* 189:556–558. <https://doi.org/10.1038/189556a0>.
109. Frye J, Karlinsky JE, Felise HR, Marzolf B, Dowidar N, McClelland M, Hughes KT. 2006. Identification of new flagellar genes of *Salmonella enterica* serovar Typhimurium. *J Bacteriol* 188:2233–2243. <https://doi.org/10.1128/JB.188.6.2233-2243.2006>.
110. Horstmann JA, Lunelli M, Cazzola H, Heidemann J, Kühne C, Steffen P, Szefs S, Rossi C, Lokareddy RK, Wang C, Lemaire L, Hughes KT, Uetrecht C, Schlüter H, Grassl GA, Stradal TEB, Rossez Y, Kolbe M, Erhardt M. 2020. Methylation of *Salmonella* Typhimurium flagella promotes bacterial adhesion and host cell invasion. *Nat Commun* 11:2013. <https://doi.org/10.1038/s41467-020-15738-3>.
111. Homma M, Fujita H, Yamaguchi S, Iino T. 1984. Excretion of unassembled flagellin by *Salmonella typhimurium* mutants deficient in hook-associated proteins. *J Bacteriol* 159:1056–1059. <https://doi.org/10.1128/jb.159.3.1056-1059.1984>.
112. Homma M, Iino T. 1985. Location of hook-associated proteins in flagellar structures of *Salmonella typhimurium*. *J Bacteriol* 162:183–189. <https://doi.org/10.1128/jb.162.1.183-189.1985>.
113. Fahrner KA, Block SM, Krishnaswamy S, Parkinson JP, Berg HC. 1994. A mutant hook-associated protein (HAP3) facilitates torsionally induced transformations of the flagellar filament of *Escherichia coli*. *J Mol Biol* 238:173–186. <https://doi.org/10.1006/jmbi.1994.1279>.
114. Bulieris PV, Shaikh NH, Freddolino PL, Samatey FA. 2017. Structure of FlgK reveals the divergence of the bacterial hook-filament junction of *Campylobacter*. *Sci Rep* 7:15743. <https://doi.org/10.1038/s41598-017-15837-0>.
115. Hong HJ, Kim TH, Song WS, Ko H-J, Lee G-S, Kang SG, Kim P-H, Yoon S-I. 2018. Crystal structure of FlgL and its implications for flagellar assembly. *Sci Rep* 8:14307. <https://doi.org/10.1038/s41598-018-32460-9>.
116. Asakura S, Eguchi G, Iino T. 1964. Reconstitution of bacterial flagella *in vitro*. *J Mol Biol* 10:42–56. [https://doi.org/10.1016/s0022-2836\(64\)80026-7](https://doi.org/10.1016/s0022-2836(64)80026-7).
117. Iino T. 1969. Polarity of flagellar growth in *Salmonella*. *J Gen Microbiol* 56:227–239. <https://doi.org/10.1099/00221287-56-2-227>.
118. Kato S, Aizawa S-I, Asakura S. 1982. Reconstruction *in vitro* of the flagellar polyhook from *Salmonella*. *J Mol Biol* 161:551–560. [https://doi.org/10.1016/0022-2836\(82\)90407-7](https://doi.org/10.1016/0022-2836(82)90407-7).
119. Renault TT, Abraham AO, Bergmiller T, Paradis G, Rainville S, Charpentier E, Guet CC, Tu Y, Namba K, Keener JP, Minamino T, Erhardt M. 2017. Bacterial flagella grow through an injection-diffusion mechanism. *Elife* 6:e23136. <https://doi.org/10.7554/eLife.23136>.
120. Hirano T, Minamino T, Macnab RM. 2001. The role in flagellar rod assembly of the N-terminal domain of *Salmonella* FlgJ, a flagellum-specific muramidase. *J Mol Biol* 312:359–369. <https://doi.org/10.1006/jmbi.2001.4963>.
121. Ohnishi K, Ohto Y, Aizawa S-I, Macnab RM, Iino T. 1994. FlgD is a scaffolding protein needed for flagellar hook assembly in *Salmonella typhimurium*. *J Bacteriol* 176:2272–2281. <https://doi.org/10.1128/jb.176.8.2272-2281.1994>.
122. Ikeda T, Asakura S, Kamiya R. 1985. “Cap” on the tip of *Salmonella* flagella. *J Mol Biol* 184:735–737. [https://doi.org/10.1016/0022-2836\(85\)90317-1](https://doi.org/10.1016/0022-2836(85)90317-1).
123. Yonekura K, Maki S, Morgan DG, DeRosier DJ, Vonderviszt F, Imada K, Namba K. 2000. The bacterial flagellar cap as the rotary promoter of flagellin self-assembly. *Science* 290:2148–2152. <https://doi.org/10.1126/science.290.5499.2148>.

124. Maki-Yonekura S, Yonekura K, Namba K. 2003. Domain movements of HAP2 in the cap-filament complex formation and growth process of the bacterial flagellum. *Proc Natl Acad Sci U S A* **100**:15528–15533. <https://doi.org/10.1073/pnas.2534343100>.
125. Song WS, Cho SY, Hong HJ, Park SC, Yoon S-I. 2017. Self-oligomerizing structure of the flagellar cap protein FliD and its implication in filament assembly. *J Mol Biol* **429**:847–857. <https://doi.org/10.1016/j.jmb.2017.02.001>.
126. Al-Otaibi NS, Taylor AJ, Farrell DP, Tzokov SB, DiMaio F, Kelly DJ, Bergeron JRC. 2020. The cryo-EM structure of the bacterial flagellum cap complex suggests a molecular mechanism for filament elongation. *Nat Commun* **11**:3210. <https://doi.org/10.1038/s41467-020-16981-4>.
127. Matsunami H, Yoon Y-H, Imada K, Namba K, Samatey FA. 2021. Structure of the bacterial flagellar hook cap provides insights into a hook assembly mechanism. *Commun Biol* **4**:1291. <https://doi.org/10.1038/s42003-021-02796-6>.
128. Nambu T, Minamino T, Macnab RM, Kutsukake K. 1999. Peptidoglycan-hydrolyzing activity of the FlgJ protein, essential for flagellar rod formation in *Salmonella typhimurium*. *J Bacteriol* **181**:1555–1561. <https://doi.org/10.1128/JB.181.5.1555-1561.1999>.
129. Cohen EJ, Hughes KT. 2014. Rod-to-hook transition for extracellular flagellum assembly is catalyzed by the L-ring-dependent rod scaffold removal. *J Bacteriol* **196**:2387–2395. <https://doi.org/10.1128/JB.01580-14>.
130. Wagner S, Diepold A. 2020. A unified nomenclature for injectisome-type type III secretion systems. *Curr Top Microbiol Immunol* **427**:1–10. https://doi.org/10.1007/82_2020_210.
131. Iino T. 1974. Assembly of *Salmonella* flagellin *in vitro* and *in vivo*. *J Supramol Struct* **2**:372–384. <https://doi.org/10.1002/jss.400020226>.
132. Minamino T, Macnab RM. 1999. Components of the *Salmonella* flagellar export apparatus and classification of export substrates. *J Bacteriol* **181**:1388–1394. <https://doi.org/10.1128/JB.181.5.1388-1394.1999>.
133. Minamino T. 2014. Protein export through the bacterial flagellar type III export pathway. *Biochim Biophys Acta* **1843**:1642–1648. <https://doi.org/10.1016/j.bbamcr.2013.09.005>.
134. Minamino T, Kawamoto A, Kinoshita M, Namba K. 2020. Molecular organization and assembly of the export apparatus of flagellar type III secretion systems. *Curr Top Microbiol Immunol* **427**:91–107. https://doi.org/10.1007/82_2019_170.
135. Claret L, Calder SR, Higgins M, Hughes C. 2003. Oligomerization and activation of the FliI ATPase central to bacterial flagellum assembly. *Mol Microbiol* **48**:1349–1355. <https://doi.org/10.1046/j.1365-2958.2003.03506.x>.
136. Minamino T, Kazetani K, Tahara A, Suzuki H, Furukawa Y, Kihara M, Namba K. 2006. Oligomerization of the bacterial flagellar ATPase FliI is controlled by its extreme N-terminal region. *J Mol Biol* **360**:510–519. <https://doi.org/10.1016/j.jmb.2006.05.010>.
137. Ibuki T, Imada K, Minamino T, Kato T, Miyata T, Namba K. 2011. Common architecture between the flagellar protein export apparatus and F- and V-ATPases. *Nat Struct Mol Biol* **18**:277–282. <https://doi.org/10.1038/nsmb.1977>.
138. Imada K, Minamino T, Tahara A, Namba K. 2007. Structural similarity between the flagellar type III ATPase FliI and F1-ATPase subunits. *Proc Natl Acad Sci U S A* **104**:485–490. <https://doi.org/10.1073/pnas.0608090104>.
139. González-Pedrajo B, Fraser GM, Minamino T, Macnab RM. 2002. Molecular dissection of *Salmonella* FliH, a regulator of the ATPase FliI and the type III flagellar protein export pathway. *Mol Microbiol* **45**:967–982. <https://doi.org/10.1046/j.1365-2958.2002.03047.x>.
140. Pallen MJ, Bailey CM, Beatson SA. 2006. Evolutionary links between FliH/YscL-like proteins from bacterial type III secretion systems and second-stalk components of the F₀F₁ and vacuolar ATPases. *Protein Sci* **15**:935–941. <https://doi.org/10.1110/ps.051958806>.
141. Imada K, Minamino T, Kinoshita M, Furukawa Y, Namba K. 2010. Structural insight into the regulatory mechanisms of interactions of the flagellar type III chaperone FliT with its binding partners. *Proc Natl Acad Sci U S A* **107**:8812–8817. <https://doi.org/10.1073/pnas.1001866107>.
142. González-Pedrajo B, Minamino T, Kihara M, Namba K. 2006. Interactions between C ring proteins and export apparatus components: a possible mechanism for facilitating type III protein export. *Mol Microbiol* **60**:984–998. <https://doi.org/10.1111/j.1365-2958.2006.05149.x>.
143. Minamino T, Morimoto YV, Hara N, Namba K. 2011. An energy transduction mechanism used in bacterial flagellar type III protein export. *Nat Commun* **2**:475. <https://doi.org/10.1038/ncomms1488>.
144. Minamino T, Morimoto YV, Kinoshita M, Aldridge PD, Namba K. 2014. The bacterial flagellar protein export apparatus processively transports flagellar proteins even with extremely infrequent ATP hydrolysis. *Sci Rep* **4**:7579. <https://doi.org/10.1038/srep07579>.
145. Minamino T, Macnab RM. 2000. FliH, a soluble component of the type III flagellar export apparatus of *Salmonella*, forms a complex with FliI and inhibits its ATPase activity. *Mol Microbiol* **37**:1494–1503. <https://doi.org/10.1046/j.1365-2958.2000.02106.x>.
146. Minamino T, Yoshimura SDJ, Morimoto YV, González-Pedrajo B, Kami-Ike N, Namba K. 2009. Roles of the extreme N-terminal region of FliH for efficient localization of the FliH-FliI complex to the bacterial flagellar type III export apparatus. *Mol Microbiol* **74**:1471–1483. <https://doi.org/10.1111/j.1365-2958.2009.06946.x>.
147. Hara N, Morimoto YV, Kawamoto A, Namba K, Minamino T. 2012. Interaction of the extreme N-terminal region of FliH with FliA is required for efficient bacterial flagellar protein export. *J Bacteriol* **194**:5353–5360. <https://doi.org/10.1128/JB.01028-12>.
148. Bai F, Morimoto YV, Yoshimura SDJ, Hara N, Kami-Ike N, Namba K, Minamino T. 2014. Assembly dynamics and the roles of FliI ATPase of the bacterial flagellar export apparatus. *Sci Rep* **4**:6528. <https://doi.org/10.1038/srep06528>.
149. Terashima H, Kawamoto A, Tatsumi C, Namba K, Minamino T, Imada K. 2018. *In vitro* reconstitution of functional type III protein export and insights into flagellar assembly. *mBio* **9**:e00988-18. <https://doi.org/10.1128/mBio.00988-18>.
150. Terashima H, Tatsumi C, Kawamoto A, Namba K, Minamino T, Imada K. 2020. *In vitro* autonomous construction of the flagellar axial structure in the inverted membrane vesicles. *Biomolecules* **10**:126. <https://doi.org/10.3390/biom10010126>.
151. Thomas J, Stafford GP, Hughes C. 2004. Docking of cytosolic chaperone-substrate complexes at the membrane ATPase during flagellar type III protein export. *Proc Natl Acad Sci U S A* **101**:3945–3950. <https://doi.org/10.1073/pnas.0307223101>.
152. Minamino T, Kinoshita M, Imada K, Namba K. 2012. Interaction between FliI ATPase and a flagellar chaperone FliT during bacterial flagellar export. *Mol Microbiol* **83**:168–178. <https://doi.org/10.1111/j.1365-2958.2011.07924.x>.
153. Minamino T, Namba K. 2008. Distinct roles of the FliI ATPase and proton motive force in bacterial flagellar protein export. *Nature* **451**:485–488. <https://doi.org/10.1038/nature06449>.
154. Paul K, Erhardt M, Hirano T, Blair DF, Hughes KT. 2008. Energy source of flagellar type III secretion. *Nature* **451**:489–492. <https://doi.org/10.1038/nature06497>.
155. Morimoto YV, Kami-Ike N, Miyata T, Kawamoto A, Kato T, Namba K, Minamino T. 2016. High-resolution pH imaging of living bacterial cells to detect local pH differences. *mBio* **7**:e01911-16. <https://doi.org/10.1128/mBio.01911-16>.

156. Minamino T, Morimoto YV, Hara N, Aldridge PD, Namba K. 2016. The bacterial flagellar type III export gate complex is a dual fuel engine that can use both H⁺ and Na⁺ for flagellar protein export. *PLoS Pathog* 12:e1005495. <https://doi.org/10.1371/journal.ppat.1005495>.
157. Minamino T, Kinoshita M, Morimoto YV, Namba K. 2021. The FlgN chaperone activates the Na⁺-driven engine of the *Salmonella* flagellar protein export apparatus. *Commun Biol* 4:335. <https://doi.org/10.1038/s42003-021-01865-0>.
158. Minamino T, Morimoto YV, Kinoshita M, Namba K. 2021. Membrane voltage-dependent activation mechanism of the bacterial flagellar protein export apparatus. *Proc Natl Acad Sci U S A* 118: e2026587118. <https://doi.org/10.1073/pnas.2026587118>.
159. Kuhlen L, Abrusci P, Johnson S, Gault J, Deme J, Caesar J, Dietsche T, Mebrhatu MT, Ganief T, Macek B, Wagner S, Robinson CV, Lea SM. 2018. Structure of the core of the type III secretion system export apparatus. *Nat Struct Mol Biol* 25:583–590. <https://doi.org/10.1038/s41594-018-0086-9>.
160. Kuhlen L, Johnson S, Zeitler A, Bäurle S, Deme JC, Caesar JJE, Debo R, Fisher J, Wagner S, Lea SM. 2020. The substrate specificity switch FlhB assembles onto the export gate to regulate type three secretion. *Nat Commun* 11:1296. <https://doi.org/10.1038/s41467-020-15071-9>.
161. Kinoshita M, Namba K, Minamino T. 2021. A positive charge region of *Salmonella* Flil is required for ATPase formation and efficient flagellar protein export. *Commun Biol* 4:464. <https://doi.org/10.1038/s42003-021-01980-y>.
162. Minamino T, Macnab RM. 2000. Domain structure of *Salmonella* FlhB, a flagellar export component responsible for substrate specificity switching. *J Bacteriol* 182:4906–4914. <https://doi.org/10.1128/JB.182.17.4906-4914.2000>.
163. Evans LDB, Poulter S, Terentjev EM, Hughes C, Fraser GM. 2013. A chain mechanism for flagellum growth. *Nature* 504:287–290. <https://doi.org/10.1038/nature12682>.
164. Abrusci P, Vergara-Irigaray M, Johnson S, Beeby MD, Hendrixson DR, Roversi P, Friede ME, Deane JE, Jensen GJ, Tang CM, Lea SM. 2013. Architecture of the major component of the type III secretion system export apparatus. *Nat Struct Mol Biol* 20:99–104. <https://doi.org/10.1038/nsmb.2452>.
165. Kawamoto A, Morimoto YV, Miyata T, Minamino T, Hughes KT, Kato T, Namba K. 2013. Common and distinct structural features of *Salmonella* injectisome and flagellar basal body. *Sci Rep* 3:3369. <https://doi.org/10.1038/srep03369>.
166. Minamino T, Macnab RM. 2000. Interactions among components of the *Salmonella* flagellar export apparatus and its substrates. *Mol Microbiol* 35:1052–1064. <https://doi.org/10.1046/j.1365-2958.2000.01771.x>.
167. Minamino T, Shimada M, Okabe M, Saijo-Hamano Y, Imada K, Kihara M, Namba K. 2010. Role of the C-terminal cytoplasmic domain of FlhA in bacterial flagellar type III protein export. *J Bacteriol* 192:1929–1936. <https://doi.org/10.1128/JB.01328-09>.
168. Bange G, Kümmerer N, Engel C, Bozkurt G, Wild K, Sinning I. 2010. FlhA provides the adaptor for coordinated delivery of late flagella building blocks to the type III secretion system. *Proc Natl Acad Sci U S A* 107:11295–11300. <https://doi.org/10.1073/pnas.1001383107>.
169. Minamino T, Kinoshita M, Hara N, Takeuchi S, Hida A, Koya S, Glenwright H, Imada K, Aldridge PD, Namba K. 2012. Interaction of a bacterial flagellar chaperone FlgN with FlhA is required for efficient export of its cognate substrates. *Mol Microbiol* 83:775–788. <https://doi.org/10.1111/j.1365-2958.2011.07964.x>.
170. Kinoshita M, Hara N, Imada K, Namba K, Minamino T. 2013. Interactions of bacterial chaperone-substrate complexes with FlhA contribute to co-ordinating assembly of the flagellar filament. *Mol Microbiol* 90:1249–1261. <https://doi.org/10.1111/mmi.12430>.
171. Inoue Y, Kinoshita M, Kida M, Takekawa N, Namba K, Imada K, Minamino T. 2021. The FlhA linker mediates flagellar protein export switching during flagellar assembly. *Commun Biol* 4:646. <https://doi.org/10.1038/s42003-021-02177-z>.
172. Fraser GM, Bennett JCQ, Hughes C. 1999. Substrate-specific binding of hook-associated proteins by FlgN and FliT, putative chaperones for flagellum assembly. *Mol Microbiol* 32:569–580. <https://doi.org/10.1046/j.1365-2958.1999.01372.x>.
173. Auvray F, Thomas J, Fraser GM, Hughes C. 2001. Flagellin polymerisation control by a cytosolic export chaperone. *J Mol Biol* 308:221–229. <https://doi.org/10.1006/jmbi.2001.4597>.
174. Bennett JCQ, Thomas J, Fraser GM, Hughes C. 2001. Substrate complexes and domain organization of the *Salmonella* flagellar export chaperones FlgN and FliT. *Mol Microbiol* 39:781–791. <https://doi.org/10.1046/j.1365-2958.2001.02268.x>.
175. Aldridge P, Karlinsey JE, Hughes KT. 2003. The type III secretion chaperone FlgN regulates flagellar assembly via a negative feedback loop containing its chaperone substrates FlgK and FlgL. *Mol Microbiol* 49:1333–1345. <https://doi.org/10.1046/j.1365-2958.2003.03637.x>.
176. Evdokimov AG, Phan J, Tropea JE, Routzahn KM, Peters HK, Pokross M, Waugh DS. 2003. Similar modes of polypeptide recognition by export chaperones in flagellar biosynthesis and type III secretion. *Nat Struct Biol* 10:789–793. <https://doi.org/10.1038/nsb982>.
177. Kinoshita M, Nakanishi Y, Furukawa Y, Namba K, Imada K, Minamino T. 2016. Rearrangements of α -helical structures of FlgN chaperone control the binding affinity for its cognate substrates during flagellar type III export. *Mol Microbiol* 101:656–670. <https://doi.org/10.1111/mmi.13415>.
178. Khanra N, Rossi P, Economou A, Kalodimos CG. 2016. Recognition and targeting mechanisms by chaperones in flagellum assembly and operation. *Proc Natl Acad Sci U S A* 113:9798–9803. <https://doi.org/10.1073/pnas.1607845113>.
179. Xing Q, Shi K, Portaliou A, Rossi P, Economou A, Kalodimos CG. 2018. Structure of chaperone-substrate complexes docked onto the export gate in a type III secretion system. *Nat Commun* 9:1773. <https://doi.org/10.1038/s41467-018-04137-4>.
180. Furukawa Y, Inoue Y, Sakaguchi A, Mori Y, Fukumura T, Miyata T, Namba K, Minamino T. 2016. Structural stability of flagellin subunit affects the rate of flagellin export in the absence of FlhS chaperone. *Mol Microbiol* 102:405–416. <https://doi.org/10.1111/mmi.13469>.
181. Minamino T, Morimoto YV, Kinoshita M, Namba K. 2021. Multiple roles of flagellar export chaperones for efficient and robust flagellar filament formation in *Salmonella*. *Front Microbiol* 12:756044. <https://doi.org/10.3389/fmicb.2021.756044>.
182. Saijo-Hamano Y, Imada K, Minamino T, Kihara M, Shimada M, Kitao A, Namba K. 2010. Structure of the cytoplasmic domain of FlhA and implication for flagellar type III protein export. *Mol Microbiol* 76:260–268. <https://doi.org/10.1111/j.1365-2958.2010.07097.x>.
183. Inoue Y, Ogawa Y, Kinoshita M, Terahara N, Shimada M, Kodera N, Ando T, Namba K, Kitao A, Imada K, Minamino T. 2019. Structural insight into the substrate specificity switching mechanism of the type III protein export apparatus. *Structure* 27:965–976.e6. <https://doi.org/10.1016/j.str.2019.03.017>.
184. Minamino T, Kinoshita M, Inoue Y, Kitao A, Namba K. 2022. Conserved GYXLI motif of FlhA is involved in dynamic domain motions of FlhA required for flagellar protein export. *Microbiol Spectr* 10:e01110-22. <https://doi.org/10.1128/spectrum.01110-22>.
185. Minamino T, Terahara N, Kojima S, Namba K. 2018. Autonomous control mechanism of stator assembly in the bacterial flagellar motor in response to changes in the environment. *Mol Microbiol* 109:723–734. <https://doi.org/10.1111/mmi.14092>.

186. Zhou J, Fazzio RT, Blair DF. 1995. Membrane topology of the MotA protein of *Escherichia coli*. *J Mol Biol* 251:237–242. <https://doi.org/10.1006/jmbi.1995.0431>.
187. Kojima S, Furukawa Y, Matsunami H, Minamino T, Namba K. 2008. Characterization of the periplasmic domain of MotB and implications for its role in the stator assembly of the bacterial flagellar motor. *J Bacteriol* 190:3314–3322. <https://doi.org/10.1128/JB.01710-07>.
188. Braun TF, Blair DF. 2001. Targeted disulfide cross-linking of the MotB protein of *Escherichia coli*: evidence for two H⁺ channels in the stator complex. *Biochemistry* 40:13051–13059. <https://doi.org/10.1021/bi011264g>.
189. Braun TF, Al-Mawsawi LQ, Kojima S, Blair DF. 2004. Arrangement of core membrane segments in the MotA/MotB proton-channel complex of *Escherichia coli*. *Biochemistry* 43:35–45. <https://doi.org/10.1021/bi035406d>.
190. Zhou J, Sharp LL, Tang HL, Lloyd SA, Billings S, Braun TF, Blair DF. 1998. Function of protonatable residues in the flagellar motor of *Escherichia coli*: a critical role for Asp 32 of MotB. *J Bacteriol* 180:2729–2735. <https://doi.org/10.1128/JB.180.10.2729-2735.1998>.
191. Che Y-S, Nakamura S, Kojima S, Kami-ike N, Namba K, Minamino T. 2008. Suppressor analysis of the MotB(D33E) mutation to probe bacterial flagellar motor dynamics coupled with proton translocation. *J Bacteriol* 190:6660–6667. <https://doi.org/10.1128/JB.00503-08>.
192. Braun TF, Poulson S, Gully JB, Empey JC, Van Way S, Putnam A, Blair DF. 1999. Function of proline residues of MotA in torque generation by the flagellar motor of *Escherichia coli*. *J Bacteriol* 181:3542–3551. <https://doi.org/10.1128/JB.181.11.3542-3551.1999>.
193. Nakamura S, Morimoto YV, Kami-ike N, Minamino T, Namba K. 2009. Role of a conserved prolyl residue (Pro-173) of MotA in the mechanochemical reaction cycle of the proton-driven flagellar motor of *Salmonella*. *J Mol Biol* 393:300–307. <https://doi.org/10.1016/j.jmb.2009.08.022>.
194. Kojima S, Imada K, Sakuma M, Sudo Y, Kojima C, Minamino T, Homma M, Namba K. 2009. Stator assembly and activation mechanism of the flagellar motor by the periplasmic region of MotB. *Mol Microbiol* 73:710–718. <https://doi.org/10.1111/j.1365-2958.2009.06802.x>.
195. Kojima S, Blair DF. 2004. Solubilization and purification of the MotA/MotB complex of *Escherichia coli*. *Biochemistry* 43:26–34. <https://doi.org/10.1021/bi0354051>.
196. Santiveri M, Roa-Eguiara A, Kühne C, Wadhwa N, Hu H, Berg HC, Erhardt M, Taylor NMI. 2020. Structure and function of stator units of the bacterial flagellar motor. *Cell* 183:244–257.e16. <https://doi.org/10.1016/j.cell.2020.08.016>.
197. Deme JC, Johnson S, Vickery O, Aron A, Monkhouse H, Griffiths T, James RH, Berks BC, Coulton JW, Stansfeld PJ, Lea SM. 2020. Structures of the stator complex that drives rotation of the bacterial flagellum. *Nat Microbiol* 5:1553–1564. <https://doi.org/10.1038/s41564-020-0788-8>.
198. Muramoto K, Macnab RM. 1998. Deletion analysis of MotA and MotB, components of the force-generating unit in the flagellar motor of *Salmonella*. *Mol Microbiol* 29:1191–1202. <https://doi.org/10.1046/j.1365-2958.1998.00998.x>.
199. Hosking ER, Vogt C, Bakker EP, Manson MD. 2006. The *Escherichia coli* MotAB proton channel unplugged. *J Mol Biol* 364:921–937. <https://doi.org/10.1016/j.jmb.2006.09.035>.
200. Morimoto YV, Che Y-S, Minamino T, Namba K. 2010. Proton-conductivity assay of plugged and unplugged MotA/B proton channel by cytoplasmic pHluorin expressed in *Salmonella*. *FEBS Lett* 584:1268–1272. <https://doi.org/10.1016/j.febslet.2010.02.051>.
201. Kojima S, Takao M, Almira G, Kawahara I, Sakuma M, Homma M, Kojima C, Imada K. 2018. The helix rearrangement in the periplasmic domain of the flagellar stator B subunit activates peptidoglycan binding and ion influx. *Structure* 26:590–598.e5. <https://doi.org/10.1016/j.str.2018.02.016>.
202. Terahara N, Kodera N, Uchihashi T, Ando T, Namba K, Minamino T. 2017. Na⁺-induced structural transition of MotPS for stator assembly of the *Bacillus* flagellar motor. *Sci Adv* 3:eaa04119. <https://doi.org/10.1126/sciadv.aao4119>.
203. Leake MC, Chandler JH, Wadhams GH, Bai F, Berry RM, Armitage JP. 2006. Stoichiometry and turnover in single, functioning membrane protein complexes. *Nature* 443:355–358. <https://doi.org/10.1038/nature05135>.
204. Lele PP, Hosu BG, Berg HC. 2013. Dynamics of mechanosensing in the bacterial flagellar motor. *Proc Natl Acad Sci U S A* 110:11839–11844. <https://doi.org/10.1073/pnas.1305885110>.
205. Tipping MJ, Delalez NJ, Lim R, Berry RM, Armitage JP. 2013. Load-dependent assembly of the bacterial flagellar motor. *mBio* 4:e00551-13. <https://doi.org/10.1128/mBio.00551-13>.
206. Castillo DJ, Nakamura S, Morimoto YV, Che Y-S, Kami-ike N, Kudo S, Minamino T, Namba K. 2013. The C-terminal periplasmic domain of MotB is responsible for load-dependent control of the number of stators of the bacterial flagellar motor. *Biophysics (Nagoya-shi)* 9:173–181. <https://doi.org/10.2142/biophysics.9.173>.
207. Pourjaberi SNS, Terahara N, Namba K, Minamino T. 2017. The role of a cytoplasmic loop of MotA in load-dependent assembly and disassembly dynamics of the MotA/B stator complex in the bacterial flagellar motor. *Mol Microbiol* 106:646–658. <https://doi.org/10.1111/mmi.13843>.
208. Kutsukake K, Ohya Y, Iino T. 1990. Transcriptional analysis of the flagellar regulon of *Salmonella typhimurium*. *J Bacteriol* 172:741–747. <https://doi.org/10.1128/jb.172.2.741-747.1990>.
209. Kutsukake K. 1997. Autogenous and global control of the flagellar master operon, *flhD*, in *Salmonella typhimurium*. *Mol Gen Genet* 254:440–448. <https://doi.org/10.1007/s004380050437>.
210. Ohnishi K, Kutsukake K, Suzuki H, Iino T. 1990. Gene *fliA* encodes an alternative sigma factor for flagellar operons in *Salmonella typhimurium*. *Mol Gen Genet* 221:139–147. <https://doi.org/10.1007/BF00261713>.
211. Ohnishi K, Kutsukake K, Suzuki H, Iino T. 1992. A novel transcriptional regulation in the flagellar regulon of *Salmonella typhimurium*: an anti-sigma factor inhibits the activity of the flagellum-specific sigma factor, σ^F . *Mol Microbiol* 6:3149–3157. <https://doi.org/10.1111/j.1365-2958.1992.tb01771.x>.
212. Hughes KT, Gillen KL, Semon MJ, Karlinsey JE. 1993. Sensing structural intermediates in bacterial flagellar assembly by export of a negative regulator. *Science* 262:1277–1280. <https://doi.org/10.1126/science.8235660>.
213. Kutsukake K. 1994. Excretion of the anti-sigma factor through a flagellar substructure couples flagellar gene expression with flagellar assembly in *Salmonella typhimurium*. *Mol Gen Genet* 243:605–612. <https://doi.org/10.1007/BF00279569>.
214. Gillen KL, Hughes KT. 1993. Transcription from two promoters and autoregulation contribute to the control of expression of the *Salmonella typhimurium* flagellar regulatory gene *flgM*. *J Bacteriol* 175:7006–7015. <https://doi.org/10.1128/jb.175.21.7006-7015.1993>.
215. Kutsukake K, Ide N. 1995. Transcriptional analysis of the *flgK* and *fliD* operons of *Salmonella typhimurium* which encode flagellar hook-associated proteins. *Mol Gen Genet* 247:275–281. <https://doi.org/10.1007/BF00293195>.
216. Ikebe T, Iyoda S, Kutsukake K. 1999. Structure and expression of the *fliA* operon of *Salmonella typhimurium*. *Microbiology (Reading)* 145:1389–1396. <https://doi.org/10.1099/13500872-145-6-1389>.
217. Wozniak CE, Chevance FFV, Hughes KT. 2010. Multiple promoters contribute to swarming and the coordination of transcription with flagellar assembly in *Salmonella*. *J Bacteriol* 192:4752–4762. <https://doi.org/10.1128/JB.00093-10>.

218. Karlinsky JE, Lonner J, Brown KL, Hughes KT. 2000. Translation/secretion coupling by type III secretion systems. *Cell* 102:487–497. [https://doi.org/10.1016/s0092-8674\(00\)00053-2](https://doi.org/10.1016/s0092-8674(00)00053-2).
219. Yokoseki T, Iino T, Kutsukake K. 1996. Negative regulation by *fliD*, *fliS*, and *fliT* of the export of the flagellum-specific anti-sigma factor, FlgM, in *Salmonella typhimurium*. *J Bacteriol* 178:899–901. <https://doi.org/10.1128/jb.178.3.899-901.1996>.
220. Kutsukake K, Ikebe T, Yamamoto S. 1999. Two novel regulatory genes, *fliT* and *fliZ*, in the flagellar regulon of *Salmonella*. *Genes Genet Syst* 74:287–292. <https://doi.org/10.1266/ggs.74.287>.
221. Aldridge C, Poonchareon K, Saini S, Ewen T, Soloyva A, Rao CV, Imada K, Minamino T, Aldridge PD. 2010. The interaction dynamics of a negative feedback loop regulates flagellar number in *Salmonella enterica* serovar Typhimurium. *Mol Microbiol* 78:1416–1430. <https://doi.org/10.1111/j.1365-2958.2010.07415.x>.
222. Galeva A, Moroz N, Yoon Y-H, Hughes KT, Samatey FA, Kostyukova AS. 2014. Bacterial flagellin-specific chaperone FliS interacts with anti-sigma factor FlgM. *J Bacteriol* 196:1215–1221. <https://doi.org/10.1128/JB.01278-13>.
223. Kutsukake K, Iino T. 1980. A *trans*-acting factor mediates inversion of a specific DNA segment in flagellar phase variation of *Salmonella*. *Nature* 284:479–481. <https://doi.org/10.1038/284479a0>.
224. Yamamoto S, Kutsukake K. 2006. FljA-mediated posttranscriptional control of phase 1 flagellin expression in flagellar phase variation of *Salmonella enterica* serovar Typhimurium. *J Bacteriol* 188:958–967. <https://doi.org/10.1128/JB.188.3.958-967.2006>.
225. Johnson RC, Bruist MF. 1989. Intermediates in Hin-mediated DNA inversion: a role for Fis and the recombinational enhancer in the strand exchange reaction. *EMBO J* 8:1581–1590. <https://doi.org/10.1002/j.1460-2075.1989.tb03542.x>.
226. Haykinson MJ, Johnson RC. 1993. DNA looping and the helical repeat in vitro and in vivo: effect of HU protein and enhancer location on Hin invertasome assembly. *EMBO J* 12:2503–2512. <https://doi.org/10.1002/j.1460-2075.1993.tb05905.x>.
227. Wang H, Tang Z, Xue B, Lu Q, Liu X, Zou Q. 2022. *Salmonella* regulator STM0347 mediates flagellar phase variation via Hin invertase. *Int J Mol Sci* 23:8481. <https://doi.org/10.3390/ijms23158481>.
228. Morimoto YV, Ito M, Hiraoka KD, Che Y-S, Bai F, Kami-Ike N, Namba K, Minamino T. 2014. Assembly and stoichiometry of FliF and FlhA in *Salmonella* flagellar basal body. *Mol Microbiol* 91:1214–1226. <https://doi.org/10.1111/mmi.12529>.
229. Fukumura T, Makino F, Dietsche T, Kinoshita M, Kato T, Wagner S, Namba K, Imada K, Minamino T. 2017. Assembly and stoichiometry of the core structure of the bacterial flagellar type III export gate complex. *PLoS Biol* 15:e2002281. <https://doi.org/10.1371/journal.pbio.2002281>.
230. Fabiani FD, Renault TT, Peters B, Dietsche T, Gálvez EJC, Guse A, Freier K, Charpentier E, Strowig T, Franz-Wachtel M, Macek B, Wagner S, Hensel M, Erhardt M. 2017. A flagellum-specific chaperone facilitates assembly of the core type III export apparatus of the bacterial flagellum. *PLoS Biol* 15:e2002267. <https://doi.org/10.1371/journal.pbio.2002267>.
231. Minamino T, Doi H, Kutsukake K. 1999. Substrate specificity switching of the flagellum-specific export apparatus during flagellar morphogenesis in *Salmonella typhimurium*. *Biosci Biotechnol Biochem* 63:1301–1303. <https://doi.org/10.1271/bbb.63.1301>.
232. Hirano T, Minamino T, Namba K, Macnab RM. 2003. Substrate specificity classes and the recognition signal for *Salmonella* type III flagellar export. *J Bacteriol* 185:2485–2492. <https://doi.org/10.1128/JB.185.8.2485-2492.2003>.
233. Kutsukake K, Minamino T, Yokoseki T. 1994. Isolation and characterization of FliK-independent flagellation mutants from *Salmonella typhimurium*. *J Bacteriol* 176:7625–7629. <https://doi.org/10.1128/jb.176.24.7625-7629.1994>.
234. Williams AW, Yamaguchi S, Togashi F, Aizawa S-I, Kawagishi I, Macnab RM. 1996. Mutations in *fliK* and *flhB* affecting flagellar hook and filament assembly in *Salmonella typhimurium*. *J Bacteriol* 178:2960–2970. <https://doi.org/10.1128/jb.178.10.2960-2970.1996>.
235. Spöring I, Martínez VA, Hotz C, Schwarz-Linek J, Grady KL, Nava-Sedeño JM, Vissers T, Singer HM, Rohde M, Bourquin C, Hatzikirou H, Poon WCK, Dufour YS, Erhardt M. 2018. Hook length of the bacterial flagellum is optimized for maximal stability of the flagellar bundle. *PLoS Biol* 16:e2006989. <https://doi.org/10.1371/journal.pbio.2006989>.
236. Minamino T, González-Pedrajo B, Yamaguchi K, Aizawa S-I, Macnab RM. 1999. FliK, the protein responsible for flagellar hook length control in *Salmonella*, is exported during hook assembly. *Mol Microbiol* 34:295–304. <https://doi.org/10.1046/j.1365-2958.1999.01597.x>.
237. Kodera N, Uchida K, Ando T, Aizawa S-I. 2015. Two-ball structure of the flagellar hook-length control protein FliK as revealed by high-speed atomic force microscopy. *J Mol Biol* 427:406–414. <https://doi.org/10.1016/j.jmb.2014.11.007>.
238. Minamino T, Saijo-Hamano Y, Furukawa Y, González-Pedrajo B, Macnab RM, Namba K. 2004. Domain organization and function of *Salmonella* FliK, a flagellar hook-length control protein. *J Mol Biol* 341:491–502. <https://doi.org/10.1016/j.jmb.2004.06.012>.
239. Moriya N, Minamino T, Hughes KT, Macnab RM, Namba K. 2006. The type III flagellar export specificity switch is dependent on FliK ruler and a molecular clock. *J Mol Biol* 359:466–477. <https://doi.org/10.1016/j.jmb.2006.03.025>.
240. Erhardt M, Hirano T, Su Y, Paul K, Wee DH, Mizuno S, Aizawa S-I, Hughes KT. 2010. The role of the FliK molecular ruler in hook-length control in *Salmonella enterica*. *Mol Microbiol* 75:1272–1284. <https://doi.org/10.1111/j.1365-2958.2010.07050.x>.
241. Erhardt M, Singer HM, Wee DH, Keener JP, Hughes KT. 2011. An infrequent molecular ruler controls flagellar hook length in *Salmonella enterica*. *EMBO J* 30:2948–2961. <https://doi.org/10.1038/emboj.2011.185>.
242. Mizuno S, Amida H, Kobayashi N, Aizawa S-I, Tate S. 2011. The NMR structure of FliK, the trigger for the switch of substrate specificity in the flagellar type III secretion apparatus. *J Mol Biol* 409:558–573. <https://doi.org/10.1016/j.jmb.2011.04.008>.
243. Minamino T, Ferris HU, Moriya N, Kihara M, Namba K. 2006. Two parts of the T3S4 domain of the hook-length control protein FliK are essential for the substrate specificity switching of the flagellar type III export apparatus. *J Mol Biol* 362:1148–1158. <https://doi.org/10.1016/j.jmb.2006.08.004>.
244. Kinoshita M, Aizawa S-I, Inoue Y, Namba K, Minamino T. 2017. The role of intrinsically disordered C-terminal region of FliK in substrate specificity switching of the bacterial flagellar type III export apparatus. *Mol Microbiol* 105:572–588. <https://doi.org/10.1111/mmi.13718>.
245. Kinoshita M, Tanaka S, Inoue Y, Namba K, Aizawa S-I, Minamino T. 2020. The flexible linker of the secreted FliK ruler is required for export switching of the flagellar protein export apparatus. *Sci Rep* 10:838. <https://doi.org/10.1038/s41598-020-57782-5>.
246. Ferris HU, Furukawa Y, Minamino T, Kroetz MB, Kihara M, Namba K, Macnab RM. 2005. FlhB regulates ordered export of flagellar components via autocleavage mechanism. *J Biol Chem* 280:41236–41242. <https://doi.org/10.1074/jbc.M509438200>.
247. Meshcheryakov VA, Kitao A, Matsunami H, Samatey FA. 2013. Inhibition of a type III secretion system by the deletion of a short loop in one of its membrane proteins. *Acta Crystallogr D Biol Crystallogr* 69:812–820. <https://doi.org/10.1107/S0907444913002102>.
248. Fraser GM, Hirano T, Ferris HU, Devgan LL, Kihara M, Macnab RM. 2003. Substrate specificity of type III flagellar protein export in *Salmonella* is controlled by subdomain interactions in FlhB. *Mol Microbiol* 48:1043–1057. <https://doi.org/10.1046/j.1365-2958.2003.03487.x>.

249. Minamino T, Inoue Y, Kinoshita M, Namba K. 2020. FliK-driven conformational rearrangements of FlhA and FlhB are required for export switching of the flagellar protein export apparatus. *J Bacteriol* 202:e00637-19. <https://doi.org/10.1128/JB.00637-19>.

250. Terahara N, Inoue Y, Kodera N, Morimoto YV, Uchihashi T, Imada K, Ando T, Namba K, Minamino T. 2018. Insight into

structural remodeling of the FlhA ring responsible for bacterial flagellar type III protein export. *Sci Adv* 4:eaa07054. <https://doi.org/10.1126/sciadv.aao7054>.

251. Kuhlen L, Johnson S, Cao J, Deme JC, Lea SM. 2021. Nonameric structures of the cytoplasmic domain of FlhA and SctV in the context of the full-length protein. *PLoS One* 16:e0252800. <https://doi.org/10.1371/journal.pone.0252800>.



Tohru Minamino received his Ph.D. in Molecular Microbiology from Hiroshima University in 1997. He then worked on the flagellar type III protein export system as a postdoctoral associate for 3 years in the laboratory of Prof. Robert M. Macnab at Yale University. He then joined the ERATO Protonic NanoMachine Project funded by the Japan Science and Technology Agency (JST) as Research Staff (1999 to 2002) and became Group Leader of the ICORP Dynamic NanoMachine Project, also funded by the JST (2002 to 2008), both of which were directed by Prof. Keiichi Namba. He has been working as an Associate Professor in the Graduate School of Frontier Biosciences at Osaka University. His main research interests include self-assembly, protein export, and energy conversion of biological nanomachines.

His main research interests include self-assembly, protein export, and energy conversion of biological nanomachines.



Miki Kinoshita received her Ph.D. in Molecular Biology from Nagoya University in 2017. She has been working as a Specially Appointed Assistant Professor in the Graduate School of Frontier Biosciences at Osaka University. Her main research interests include the structures and functions of biological supramolecular assemblies.